CHARACTERISTICS OF PULSATING FLOWS IN A PULSE COMBUSTOR TAILPIPE

A Thesis
Presented to
The Academic Faculty

by

Wichit Liewkongsataporn

In Partial Fulfillment
of the Requirements for the Degree
Master of Science in the
Woodruff School of Mechanical Engineering

Georgia Institute of Technology
August 2006

CHARACTERISTICS OF PULSATING FLOWS IN A PULSE COMBUSTOR TAILPIPE

Approved by:

Dr. Timothy Patterson, Advisor
School of Mechanical Engineering
Georgia Institute of Technology

Dr. Frederick W. Ahrens
School of Mechanical Engineering
Georgia Institute of Technology

Dr. Cyrus K. Aidun
School of Mechanical Engineering
Georgia Institute of Technology

Date Approved: June 23, 2006

ACKNOWLEDGEMENTS

I wish to thank Dr. Tim Patterson for encouraging me to write up this thesis and giving me direction to stay on track. I would like to specially thank Dr. Fred Ahrens for guidance and suggestions of fundamentals I have learned along with this project. I would like to thank Jim Loughran for the help with experiments of a pulse combustor. In addition, I would like to thank all of them for helping me learn and improve my writing skill through publications during the course of study and research.

I am grateful to the Institute of Paper Science and Technology for recruiting and supporting me since the beginning of my study in the US. Finally, I would like to thank Engineering Computing Services (ECS) for making FLUENT and GAMBIT software available and Partners for the Advancement of Collaborative Engineering Education (PACE) for providing the software license through ECS.

TABLE OF CONTENTS

LIST OF TABLES

Page

LIST OF FIGURES

Page

LIST OF SYMBOLS

Letter Symbols

c	Speed of Sound
c_p	Specific Heat (Constant Pressure)
c_v	Specific Heat (Constant Volume)
D	Tailpipe Diameter
E	Specific Total Energy
f	Frequency
h	Specific Enthalpy
$\bar{\bar{I}}$	Unit Tensor
k	Thermal Conductivity
L	Tailpipe Length
MW	Molecular Weight
p	Static Pressure (Absolute)
p_t	Total Pressure (Gauge)
Pr	Prandtl Number
r	Radial Position
R	Gas Constant
$\overline{R}$	Universal Gas Constant
Re	Reynolds Number
t	Time
T	Temperature
u	Axial Velocity

$\bar{V}$	Volume Ratio (Combustion Chamber/Tailpipe)
Wo	Womersley Number
x	Axial Distance along the Tailpipe

Greek Symbols

γ	Specific Heat Ratio
λ	Acoustic Wavelength
μ	Dynamic Viscosity
ν	Kinematic Viscosity
ρ	Density
τ	Normalized Cycle Time
$\bar{\bar{\tau}}$	Stress Tensor
$\vec{\upsilon}$	Velocity Vector
ω	Radian Frequency

Subscripts

0	Rest State of Flow
a	Ambient or Atmospheric
A	Amplitude
b	Bulk-Flow Averaged
f	Change from Rest State
m	Mean or Time-Averaged
t	Turbulent

SUMMARY

Pulsating flows in a Helmholtz pulse combustor tailpipe were numerically simulated by a commercial CFD software package, FLUENT. The effects of ambient temperature on the characteristics of the pulsating tailpipe flows were studied. Two study cases, with high and low levels of ambient temperature, were simulated with compressible flow equations. An additional case, with high ambient temperature, was simulated with "incompressible" (temperature-dependent density) flow equations. Results showed that the effect of ambient temperature on the mean temperature profile in the tailpipe was limited to the distance where the ambient fluid traveled into the tailpipe during the period of flow reversal. In this region, the amplitude of mass flow rate oscillation significantly increased, due to higher density associated with low ambient temperature. The overall effects of cooler ambient temperature included an increase in mean pressure at the entrance of the tailpipe and a decrease in the magnitude of velocity amplitude profile along the tailpipe. Interestingly, the mean velocities along the tailpipe, even at the tailpipe exit, were not affected by the cooler ambient air. The mean velocity at the exit corresponded to the higher temperature of fresh fluid from upstream, which was not affected by the ambient temperature, driven out of the tailpipe in each oscillation cycle. The linear acoustic theory with appropriate assumptions could be used to calculate the magnitude of the profiles of velocity amplitude along the tailpipe as a fair approximation, at least for the study cases in this thesis.

CHAPTER 1

INTRODUCTION

Motivation and Significance

Pulse combustors have been used to enhance heat transfer in industrial heating and drying applications, for example, household heating units, furnaces, spray dryers, flash dryers, and fluid-bed dryers (Zinn, 1996, Kudra & Mujumdar, 2002). As for impingement drying application, significant improvement in impingement heat transfer by a pulsating jet from a pulse combustor tailpipe has been experimentally demonstrated by Eibeck et al. (1993). The enhancement factor, compared to steady jet impingement, was as high as 2.5. Nevertheless, an industrial impingement drying system with a pulse combustor has never been reported in spite of the potential of this system. This was the motivation for a project called Pulsed Air Drying (PAD) at the Institute of Paper Science and Technology (IPST) at The Georgia Institute of Technology.

The ultimate goal of this project is to develop a commercial impingement drying system equipped with a pulse combustor and a multiple-nozzle system for drying paper or similar materials. No such system currently exists. Constant-velocity jet impingement drying hoods are conventionally used in Yankee dryers for tissue and towel paper manufacturing processes. As for other paper grades, such as newsprint, printing and writing paper, or paperboard, impingement drying systems have proposed as a method to increase the drying rate of the conventional drying system, a series of steam-heated cylinders (Pikulik, 1994). An impingement dryer could be combined with the steam-heated dryer by installing it above the cylinder similar to a Yankee dryer, or by installing

the impingement system between two cylinders as with the Optidry Vertical produced by Metso Paper.

The first step of the PAD project is the investigation of a potential enhancement factor for impingement drying or heat transfer by a pulsating jet as compared to a steady jet in a configuration similar to practical impingement drying systems. In Eibeck et al. (1993), the configuration was quite different from industrial drying systems, i.e., a single nozzle (tailpipe) with unconfined impingement vs. an array of nozzles with confined impingement. In addition, the reported results were based on only one operating condition of the pulsating jet, i.e., mean mass flow rate, frequency, temperature, and velocity amplitude ratio. The parameter of interest in this thesis is the velocity amplitude ratio, defined as the ratio between the amplitude of velocity oscillation and the mean velocity. It is of interest because it is directly related to the heat transfer enhancement factor as shown by Liewkongsataporn et al. (2006a). In the work of Eibeck et al. (1993), the amplitude of the velocity oscillation was calculated from a simplified one-dimensional momentum equation which assumed incompressible or solid-plug flow in the tailpipe. Given the importance of the velocity amplitude ratio with respect to evaluating drying performance, it is necessary to verify the accuracy of the calculation method.

The velocity oscillation in the tailpipe is difficult to experimentally measure unless a sophisticated system such as laser Doppler velocimetry is used. Therefore, during the preliminary investigation of the PAD project, the velocity oscillation will be approximated based on simplifying assumptions such as the linear acoustic theory or solid-plug flow oscillation. In the experiments of pulsating heat transfer or drying, a

common practice is plotting the enhancement factor against the velocity amplitude ratio. This plot would give an idea of how high the velocity amplitude ratio should be for a significant improvement of an impingement drying system. Therefore, the accuracy of this parameter is important for the feasibility of the project. An objective of this thesis is to evaluate approximation methods for determining the velocity amplitude ratio, compared with "more exact" results from numerical simulations.

The PAD project includes the investigation of the mechanism of heat transfer enhancement, the design of a pulse combustor with various types of nozzle arrays, and the study of the effects of multiple parameters on drying performance. These parameters include the separation distance between the nozzle and the surface, the frequency of the oscillation, types of nozzles, the configuration of nozzle arrays, the temperature of the jet, the speed of the surface, and the initial moisture ratio of the material. A full range of laboratory experiments would require considerable time and resources. Numerical simulation is an effective tool to achieve the goal of the project. As the numerical simulation is a main tool for the study in this thesis, another objective of the thesis is to preliminarily assess the accuracy of results from the numerical simulation for pulsating flows produced by pulse combustors.

Objectives

The main objective of the thesis is to study the characteristics of pulsating flows in the tailpipe of a Helmholtz pulse combustor in response to specified combustion chamber pressure oscillation amplitude and frequency. More specifically, the thesis focuses on the characteristics of bulk properties of the main flow variables, i.e., velocity, temperature, and pressure, with the objective of comparing the results of a full CFD

model with solutions from simplified equations. As mentioned earlier, the velocity amplitude ratio is the parameter of interest. This parameter is the ratio of two quantities: the amplitude of velocity oscillation and the time-averaged velocity. It is expected that the numerical simulation would provide solutions that lead to validation of simpler ways to estimate those two quantities.

The work in this thesis is based on CFD simulation, which will also be used as a tool for the study of pulsating jet impingement flows in the PAD project. Hence, another objective of the thesis is to evaluate overall accuracy of the simulation with a simplified computational domain and boundary conditions. The simulation results of a study case will be compared to previously published experimental data as the validation case.

Scope and Study Cases

The numerical simulation in this thesis is performed using a commercial CFD software package, FLUENT. The reference data for pulse combustor tailpipe flows are from published experimental results produced at the Combustion Research Facility, Sandia National Laboratories, Livermore, California (Dec et al., 1991, Dec & Keller, 1990, and Dec & Keller, 1989). The data that will be used for the validation of the simulation are the oscillation of velocity and temperature at various positions along the tailpipe. Other data in those publications include wall shear stress and wall heat flux as well as the effects of pulse combustor conditions on these parameters. However, the scope of the study in the thesis is limited to main flow variables, i.e., velocity, temperature, and pressure. Furthermore, the study focuses on cross-sectional averaged or bulk characteristics of these flow variables so that the results could be compared with simplified one-dimensional solutions. Another limitation is that the flows in the

simulation are assumed axisymmetric although the reference data showed some behavior of a secondary flow as a result of three-dimensional geometry, i.e., a square cross-sectional tailpipe.

In order to have at least two sets of data for the evaluation of simplified models, two study cases are simulated. The variable is the temperature of the ambient air around the tailpipe. The first case, as the validation case with operating conditions similar to the reference data, has a higher temperature, and the second case has a lower temperature. Another reason for selecting these two cases, or this variable, is that preliminary experiments on jet impingement heat transfer have been run with confined and unconfined impingement conditions (Liewkongsataporn et al., 2006b). Typically, the temperatures around the exit of the tailpipe are significantly different between the two conditions. The temperature around the tailpipe exit in a confined impingement zone is as high as the temperature of the exiting jet, whereas the temperature around the tailpipe exit for unconfined impingement is as low as room ambient temperature. These two cases are simulated with a fully-compressible flow model, in which the density is assumed to follow the ideal gas law. In addition to these two cases, another case is simulated with an "incompressible" flow model, in which the density is assumed to be temperature-dependent only, and with the same (high) ambient temperature as the first case. The third simulation case is run in order to test whether the "incompressible" flow assumption is physically reasonable for pulsating tailpipe flows produced by pulse combustors.

CHAPTER 2

LITERATURE REVIEW

Pulse Combustion Process

Pulse combustion is a self-sustained and self-oscillating process driven by combustion, coupling with resonant oscillation of the flow in the tailpipe. Three types of pulse combustor exist, i.e., Helmholtz, Schmidt, and Rijke tubes (Zinn, 1996, Kudra & Mujumdar, 2002). The pulse combustor at Sandia National Laboratories was a Helmholtz type, which consisted of a combustion chamber and a tailpipe. Typically, the combustion chamber of a Helmholtz pulse combustor is a "closed" end with a larger diameter and a larger volume than the tailpipe. A main component of a pulse combustor is unidirectional supply valves for reactants, i.e., air and fuel. The reactants could be pre-mixed in a mixing chamber prior to entering the combustion chamber or separately fed to the combustion chamber. The operation of a unidirectional supply valve for a pulse combustor is based on pressure differential across the valve, i.e., between pressure in the supply lines and pressure in the combustion chamber or the mixing chamber. When the pressure in the chamber is lower than the supply pressure, the valves open and reactants enter. When the pressure in the chamber is higher the valves close. Thus, the reactants are allowed to flow only in one direction, i.e., into the chamber. The timing of the flow is controlled by the combustion chamber pressure. There are several types of unidirectional valves: flapper valves, rotary valves, and aerodynamic valves. For the experiments at Sandia National Laboratories, a flapper valve was used.

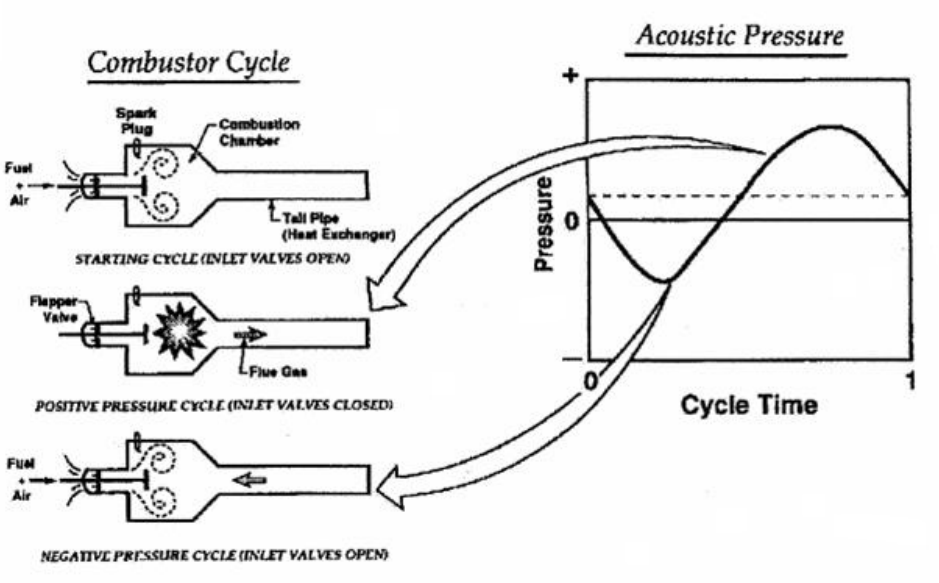

Figure 2.1: Helmholtz pulse combustion cycle (Keller et al., 1993)

A typical cycle of self-sustained process of pulse combustion is shown in Figure 2.1. Initially, a heat source such as a spark plug is required to initiate the "explosion" when reactants initially flow through flapper valves into the combustion chamber. The reaction between fuel and air causes a sudden increase in combustion chamber pressure, which subsequently causes the flapper valves to close. Flue gas from the reaction flows out of the combustion chamber and through the tailpipe. Then the combustion chamber pressure decreases. When the pressure level is lower than supply pressure of fuel and air, the flapper valves open again. Fresh reactants flow into the combustion chamber. At the same time, hot flue gas in the tailpipe starts to slow down and eventually flows back toward the combustion chamber if the pressure stays low long enough. At some point, well-mixed fresh reactants combined with heat from remaining or flow-reversing flue gas causes another "explosion" to start a new cycle. This process repeats itself over and over again. The pressure oscillation parameters, i.e., the amplitude and the frequency, depend

on several factors such as the geometry and the dimension of the pulse combustor, the equivalence ratio of the reactants, and the type and size of valves.

The steady oscillation of pulse combustion follows the well-known Rayleigh criterion, which requires the phase difference between pressure oscillation and heat release process in the combustion chamber be less than a quarter of the cycle (Zinn, 1996). In this case, the heat release process is from the reaction between reactants. The timing of the reaction depends on the flow path (mixing rate) of reactants, which is determined by the design of the combustion chamber (Keller and Barr, 1996).

Pulsating Flows in a Pulse Combustor Tailpipe

The simulation in this thesis is largely based on measurement data from pulse combustor experiments at Sandia National Laboratories (Dec et al., 1991, Dec & Keller, 1990, Dec & Keller, 1989). Hence, this part of the literature review focuses on those experimental results. The tailpipe of the pulse combustor in these experiments was a square cross-sectioned tailpipe with clear-glass walls for data acquisition purpose. The exit of the tailpipe was connected to a decoupling chamber, a large-diameter tank. Therefore, ambient temperature around the tailpipe exit was not as low as room temperature. Around the tailpipe walls, cooling air was fed as in a counter-flow heat exchanger. Several tailpipe lengths and operating parameters, such as mass flow rate and equivalence ratio, were varied in the experiments. However, a case with relatively high oscillation amplitude of pressure and velocity was taken as a base case. The measurement data employed in this thesis were based on this base case.

The base case had an 880-mm long tailpipe with a mean mass flow rate of about 4 g/s and a mean Reynolds number of 3750. The RMS value of pressure amplitude in the

combustion chamber was 7.4 kPa. The authors approximated the Helmholtz pulse combustor as a Schmidt type (or quarter-wave tube) with variable cross-sectional area and applied the acoustic theory to estimate pressure and velocity profiles at their maximum oscillation along the tailpipe as shown in Figure 2.2. Although these plots might be qualitatively accurate, the quantitative accuracy needs to be verified.

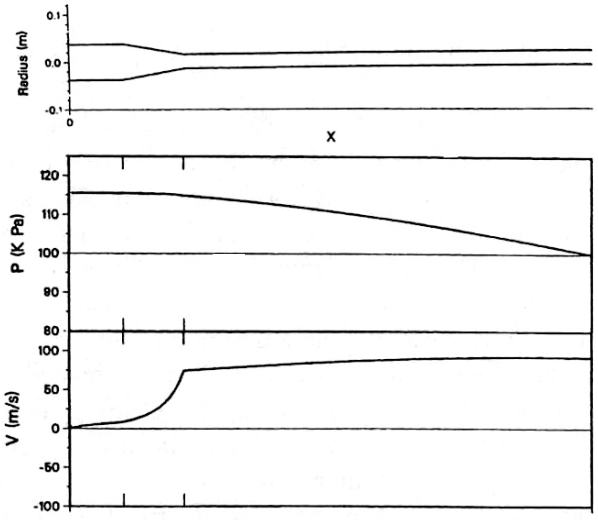

Figure 2.2: Pressure and velocity amplitude profiles at their maximum values in a Helmholtz pulse combustor (Dec et al., 1991)

The velocity oscillation in the tailpipe was measured using the laser Doppler velocimetry technique. The presented results were ensemble-averaged. Figure 2.3 shows a plot of velocity oscillation at the center of the tailpipe at the base location, 540 mm from the tailpipe entrance, along with pressure oscillation in the combustion chamber. As predicted by the momentum equation, the phases of the pressure and velocity oscillations differ by about a quarter of a cycle. The pattern of oscillation, especially the combustion chamber pressure, could be assumed sinusoidal.

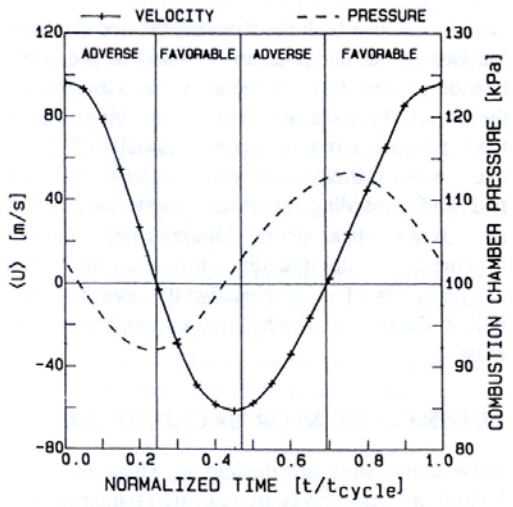

Figure 2.3: Combustion chamber pressure and tailpipe velocity oscillation in a Helmholtz pulse combustor tailpipe (Dec et al., 1991)

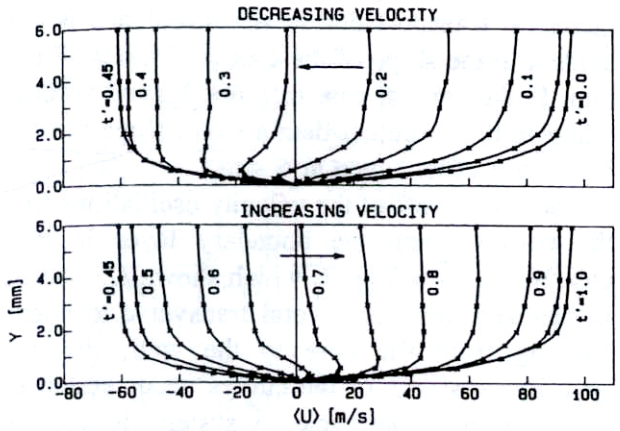

Figure 2.4: Instantaneous velocity profiles across the tailpipe at the base location, x = 540 mm (Dec et al., 1991)

Figure 2.4 shows instantaneous velocity profiles at the base location. Boundary layer thickness was limited to about 2 mm. Within the boundary layer, the momentum of fluid was less than that far away from the wall, resulting in a phase lead of velocity oscillation in this region with respect to bulk flow. This behavior was the same as

predicted by analytical solutions of laminar pulsating flows. However, the difference between turbulent and laminar flow was in the profiles of maximum or minimum velocities. There were overshoots at the edge of boundary layers of laminar flows, whereas in turbulent flows as shown in Figure 2.4, the profiles were smooth from the wall to the bulk as a result of greater dissipation of turbulence.

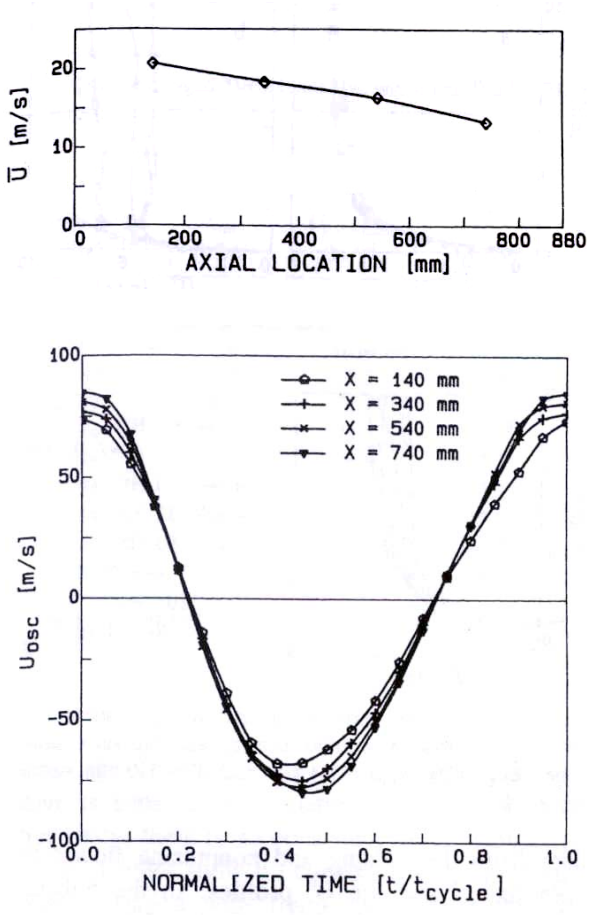

Figure 2.5: Mean and oscillating part of velocity along the tailpipe center (Dec et al., 1991)

Figure 2.5 shows mean velocity and velocity amplitude at four positions along the center of the tailpipe. The mean velocity decreased due to heat loss to the wall. The

amplitude of the velocity oscillation increased toward the end of the tailpipe. Another feature was that the oscillation near the exit was more symmetric than the upstream oscillation. Although these amplitudes were not much different, the increasing trend implied the behavior of a compressible flow. Despite this behavior, in later work, Keller et al. (1993) and Eibeck et al. (1993) assumed that the pulsating tailpipe flow generated by pulse combustion behaved like an incompressible solid-plug flow and calculated velocity oscillation with a simplified momentum equation. This later work dealt with pulsating jet characteristics and impingement heat transfer and used a pulse combustor with a round tailpipe without cooling air around the wall and without a decoupling tank.

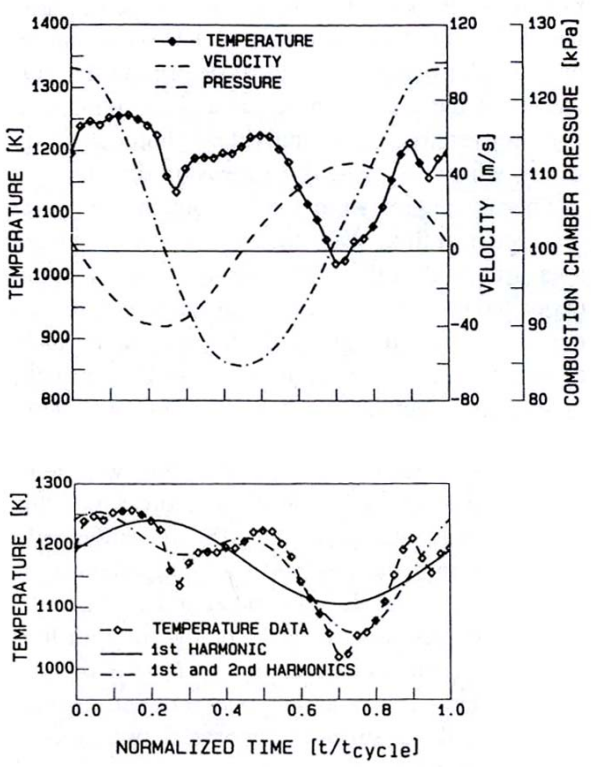

Figure 2.6: Temperature oscillation in the tailpipe at the base location, x = 540 mm (Dec & Keller, 1990)

Figure 2.6 shows the plot of temperature oscillation at the base location together with combustion chamber pressure and tailpipe velocity oscillation. There were sudden drops in temperature when the flow changed direction. This was in accordance with the increase of wall heat flux at those points in time, according to the authors, possibly caused by secondary flows. If this was the case, this kind of behavior would not be expected in simulation results in this thesis due to axisymmetry. The bottom part of Figure 2.6 shows the harmonics of temperature plots. The first harmonic had a quarter-cycle phase shift with respect to the velocity oscillation. The temperature (1st harmonic) reached the maximum value, from higher-temperature fluid upstream, when the flow changed direction from positive to negative, and vice versa. Figure 2.7 shows temperature plots at three locations along the tailpipe. Mean temperature decreased due to heat loss at the walls to the cooling air around the tailpipe.

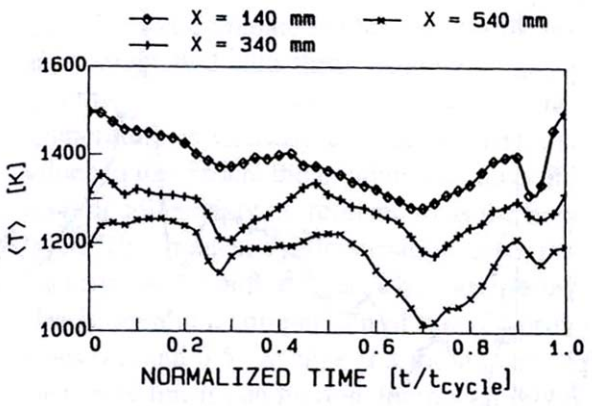

Figure 2.7: Temperature oscillation along the tailpipe center (Dec & Keller, 1990)

In another set of experiments at Sandia National Laboratories, a pulse combustor with a round tailpipe was used for studying characteristics of a pulsating jet exiting the tailpipe (Keller et al., 1993) and impingement heat transfer enhancement (Eibeck et al., 1993). The length of the tailpipe was 880 mm and the diameter was 50 mm. Combustion chamber pressure amplitude was about 10 kPa, and mean mass flow rate was about 9 g/s. In this condition, from the diagram in the publication, there was no cooling air around the tailpipe and no decoupler at the end of the tailpipe. Hence, the temperature of the gas in the tailpipe was still high but ambient air was at room temperature. Figure 2.8 shows the plot of temperature cycle at a distance of one half tailpipe diameter outside the tailpipe exit. The peak value indicated the temperature of flue gas from further inside the tailpipe. The minimum value indicated ambient temperature drawn back into the tailpipe during flow reversal.

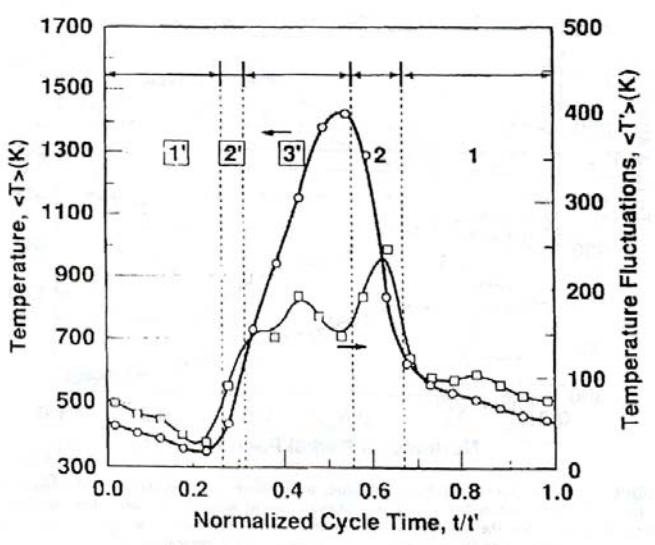

Figure 2.8: Temperature oscillation near the exit of the tailpipe (Keller et al., 1993)

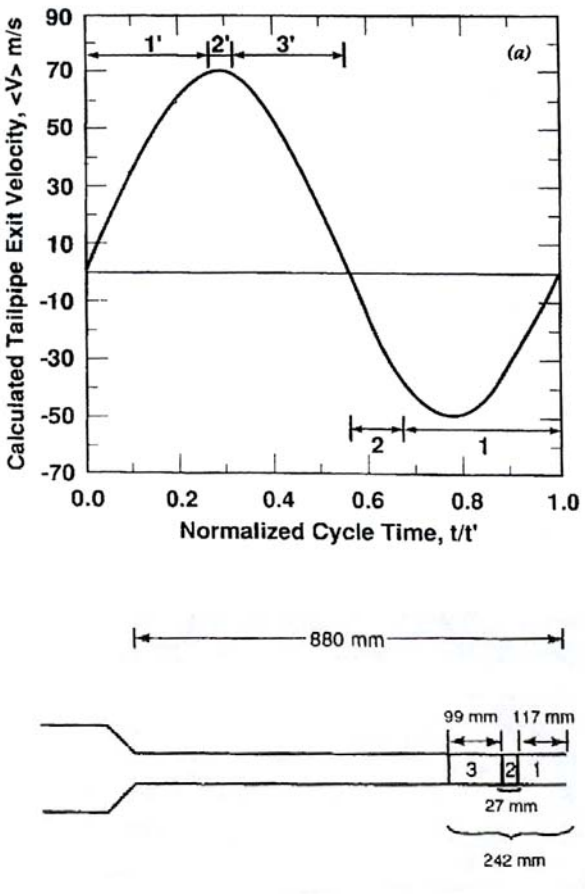

Figure 2.9: Calculated velocity oscillation in the tailpipe (Keller et al., 1993)

The temperature cycle in Figure 2.8 was sectioned into five parts, numbered 1, 2, 1′, 2′, and 3′. These sections correspond with the numbered sections for the calculated velocity cycle in Figure 2.9. Starting with section 2, at the beginning of flow reversal, part of the exiting jet of the previous cycle was drawn back into the tailpipe. Thus, the temperature was still high but decreasing. At the beginning of section 1, the exiting jet was cut off by ambient air entering the tailpipe exit as a "line sink flow." The temperature remained low in section 1 as ambient air continued to flow in. As the flow started to change direction again, fluid particles of ambient air in section 1 were the first part to

flow out of the tailpipe (section 1′), followed by fluid from section 2 (section 2′). Finally, fresh hot gas from upstream flow (section 3′) was driven out of the tailpipe.

In these experiments, the velocity oscillation was not experimentally measured. The plot in Figure 2.9(*a*) was calculated from the assumption that the combustion chamber of the Helmholtz pulse combustor had relatively larger volume than the tailpipe. Thus, the pulsating flow in the tailpipe was assumed to behave as an oscillating solid-plug flow. (This is essentially the behavior of a Helmholtz resonator, where the neck is typically much smaller than the container.) Therefore, a simplified momentum equation was used to calculate velocity oscillation amplitude from pressure amplitude in the combustion chamber and space- and time-averaged density. The question is, as the main motivation for this thesis, how accurate was the plug-flow approximation? There are two parts of this velocity calculation: the time-averaged value and the amplitude of oscillation. The time-averaged or mean velocity, as details were not given in the publication, could be simply calculated from the mean mass flow rate and mean temperature. However, in the case with low ambient temperature, the mean temperature would sharply drop in the region near the exit because the distance traveled by the reversing-flow fluid is limited as shown in Figure 2.9(*b*). Therefore, the calculation of mean velocity from mean temperature might not be accurate for this case. Likewise, the velocity amplitude might not be simply calculated from the solid-plug flow assumption, or even with the linear acoustic theory, due to an underlying assumption that the change in density is very small. Therefore, fully compressible flow equations should be used to justify these simplifying assumptions.

Basic Pulsating Flow Characteristics

There have been numerous studies about pulsating flows, both external and internal flows. However, few researchers have studied flows with similar characteristics to pulse combustor tailpipe flows, i.e., large amplitude ratio causing flow reversal, high oscillation frequency, turbulence, and, in some cases, large variation in temperature. The purposes of these studies also vary. Nevertheless, a few studies will be reviewed for some basic characteristics of pulsating internal flows.

Analytical solutions for pulsating laminar flows are available for various conditions, for example, external flow with an oscillating wall and oscillating channel and pipe flows (Schilichting & Gersten, 2000), and a flow induced by oscillating mass flow rate in a circular tube (Unsal et al., 2005). A common feature of these flows is the dependence of the velocity profile on the frequency of the oscillation. When the frequency is very low, instantaneous velocity profiles remain parabolic similar to a steady flow, and there is a limited phase shift between pressure and velocity oscillations. When the frequency is high enough, velocity profiles become flatter, the phase shift between pressure and velocity is a quarter of a cycle, and there is always overshoot at the edge of boundary layers in velocity profiles. For internal flows, the frequency of the oscillation is a part of an important dimensionless parameter in the exact solutions, the Womersley number, $Wo \equiv R\sqrt{\omega/\nu}$, where R is the radius of a pipe or the half height of a channel.

The characteristics of internal turbulent pulsating flows are similar to laminar flows in terms of the dependence of characteristics on the oscillation frequency. Scotti & Piomelli (2001) used direct numerical simulation (DNS) and large-eddy simulation (LES) to study turbulent pulsating flows in a channel without flow reversal. At low and

intermediate frequencies, the outer layer (bulk flow) and the inner layer (near the wall) were coupled, whereas at high frequencies, the bulk flow behaved like an oscillating plug flow and unsteadiness was limited to within boundary layers. The response of turbulent quantities such as turbulent kinetic energy also depended on the frequency. At high frequencies, the response is at the same frequency, whereas at low and intermediate frequencies, the response showed some nonlinear behavior and higher harmonic components.

Another parameter of pulsating flows that has been studied by several research groups is wall shear stress. In Dec et al. (1991), pulsating wall shear stresses were calculated from velocity profiles and the viscosity evaluated at a wall temperature. It was found that the mean wall shear stress of pulsating flows at the base location was only slightly greater than that of steady flows calculated from a correlation at the same mean Reynolds numbers. Manna and Vacca (2005) used an LES model to simulate pulsating pipe flows with large amplitude ratios causing flow reversal. Results showed a reduction in flow resistance compared to steady flows with same mean Reynolds numbers. Lodahl et al. (1998) experimentally studied pulsating flows over wider range of mean Reynolds numbers and velocity amplitude ratios. The mean wall shear stresses of pulsating flows could be equal to, less than, or greater than the wall shear stresses of steady flows, depending on flow regime. If the amplitude ratio was less than one, the flow was called "current dominated." And, if the amplitude ratio was greater than one, the flow was called "wave dominated." There was also a region where both "current" and "wave" were equally significant, i.e., at amplitude ratio around one. At all ranges of Reynolds number tested, the current-dominated flows had the same wall shear stress as steady flows. Wave-

dominated flows had multiple characteristics. At low Reynolds numbers (< 27,000), mean wall shear stress became slightly less than steady wall shear stress when the amplitude ratio was slightly greater than one. When the amplitude ratio increased to a threshold value, mean wall shear stress was significantly greater than steady wall shear stress. At high Reynolds numbers, no reduction in wall shear stress was observed. At amplitude ratios slightly greater than one, mean wall shear stress was still equal to steady wall shear stress. At amplitude ratios greater than a threshold value, mean wall shear stress was greater than steady wall shear stress. These published data were somewhat inconsistent, suggesting that future work is needed.

Heat Transfer Enhancement by Pulsating Flows

Internal pulsating flows have been of interest as a technique for heat transfer enhancement. It has been shown experimentally and numerically that pulsating flows, with large velocity oscillation amplitudes resulting in flow reversal, could increase wall heat transfer compared to steady flows. This advantage is the main motivation for applying pulsating flows to industrial drying applications. However, in this thesis, heat transfer enhancement (and wall shear stress) is not the main objective. Only a few publications about this subject are briefly reviewed here.

Hanby (1969) used a Schmidt pulse combustor for an experimental study. Heat flux at several positions on the wall of the tailpipe was measured. The enhancement factor was plotted against velocity amplitude ratio, calculated from the linear acoustic theory of a quarter-wave tube, for each position. A quasi-steady theory was also applied to a correlation of Nusselt number for a circular tube to obtain a time-averaged value from a pulsating flow. The results of heat transfer enhancement from the quasi-steady

theory were in agreement with measured data. When the amplitude ratio was less than one, no enhancement or slightly less heat transfer occurred. When the amplitude ratio was greater than one, the local enhancement factor was roughly about half the value of the local amplitude ratio.

Dec and Keller (1989) experimentally varied several parameters of Helmholtz pulse combustors to study the dependence of heat transfer on pulsating flow characteristics. The Nusselt number for the pulsating flow (the base case) was time- and space-averaged from data shown in Figure 2.10. The enhancement factor with respect to the steady flow was about 2.5, which was also in agreement with the data in Hanby (1969), as the amplitude ratio was about 5. Moreover, from a parameter study, the heat transfer enhancement factor was found to be a function of two parameters, the product of frequency and velocity amplitude and the velocity amplitude ratio. It was also found that the frequency must be above some threshold frequency for enhancement to occur.

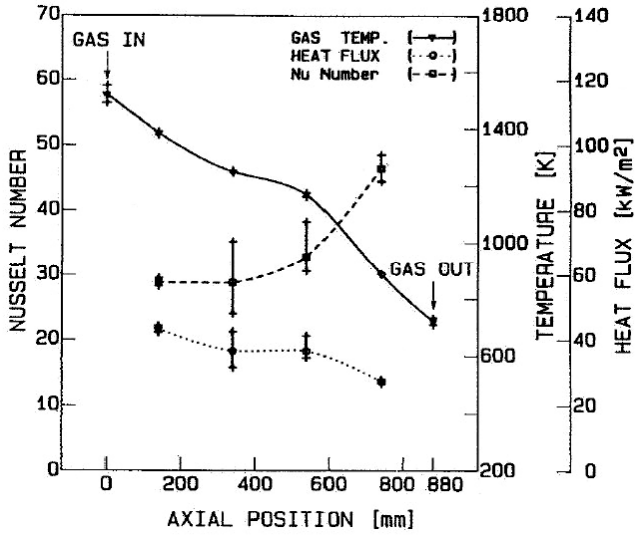

Figure 2.10: Wall heat transfer along the tailpipe (Dec & Keller, 1989)

Wang and Zhang (2005) numerically studied heat transfer enhancement of incompressible pulsating flow in a pipe with CFD simulation. The turbulence model used was a low-Reynolds-number k-ε model. Flow conditions for comparison were considered hydrodynamically and thermally fully-developed because a large ratio (200) between the length and the radius of the pipe was used for a computational domain. The plot of enhancement factor against the amplitude ratio was similar to that in Hanby (1969). However, it was found that the enhancement also depended on another parameter, Womersley number. At the same amplitude ratios, maximum heat transfer enhancement occurred at Wo = 40-50.

Acoustic Resonance Solutions

In Hanby (1969), the pulse combustor was a Schmidt type, therefore the calculation of velocity amplitude was accomplished by assuming a standing quarter wave of pressure, in which the maximum pressure was at the inlet or closed end of the tailpipe then decreasd sinusoidally to atmospheric pressure at the exit or open end. From the linear wave equation, the pattern of velocity amplitude was simply opposite to that of pressure, i.e., it started from zero at the closed end and increased sinuosidally to its maximum at the open end. For a special case, with heat loss at the wall, Sujith et al. (1995) derived the solutions of acoustic resonance for a linear axial temperature gradient in a Schmidt tube.

However, the configuration of a Helmholtz pulse combustor is different from a Schmidt pulse combustor. The combustion chamber of Helmholtz type usually has a larger diameter and volume than the tailpipe. Hence, at the entrance of the tailpipe, the velocity amplitude should not to be zero, as shown in Figure 2.2. The quarter-wave tube

solution is not valid for the tailpipe of a Helmholtz pulse combustor. Ahrens (1979) solved a linear wave equation with an appropriate boundary condition at the entrance of the tailpipe, i.e., mass conservation between the combustion chamber and the flow at the tailpipe entrance. The solutions of pressure and velocity oscillation profiles were general enough to cover from one limit, i.e., a Schmidt tube ($\overline{V} = 0$), to another limit, i.e., a Helmholtz resonator with an incompressible flow ($\overline{V} \to \infty$). Details of the derivation of the solutions are given in the Appendix. These solutions will be tested with the results from CFD simulation later in Chapter 4.

CHAPTER 3

NUMERICAL SIMULATION

The numerical simulation in this thesis is performed using FLUENT version 6.2. The grid cells in the computational domain are generated by the software package GAMBIT version 2.2. CFD simulations in FLUENT employ a control-volume-based method with efficient numerical techniques such as the Gauss-Seidel algorithm and a multigrid method. FLUENT provides numerous options for numerical schemes and models for wide ranges of flows. Pulsating flows in this thesis could be considered simple in terms of flow geometry and single-phase flow. However, pulsating flows in pulse combustor tailpipes are also complex flows in terms of unsteadiness, turbulence, and adverse pressure gradients. The governing equations consist of the three basic conservation equations for a Newtonian fluid, one equation of state, and a turbulence model. The computational domain and boundary conditions are designed such that the simulation remains simple but still captures main flow characteristics of the experimental data in the reference, i.e., Dec et al., 1991 and Dec & Keller, 1990. The fluid for the flows in the simulations is assumed to be air for convenience. In the reference, pure methane and air with an equivalence ratio of one, or a stoichiometric mixture, were used as the reactants. The exhaust gas from the combustion was, assuming a complete reaction, 210 parts of nitrogen, 36 parts of water vapor, and 44 parts of carbon dioxide, on a mass basis. As the amount of nitrogen was about 72% by mass of the exhaust gas, using air properties should not significantly compromise the results.

Governing Equations

As the study cases are turbulent flows, the governing equations for the simulation are Reynolds-Averaged Navier-Stokes (RANS) equations. Extra terms in the momentum equations are so-called Reynolds stresses. These terms are modeled, by most turbulence models, with the Boussinesq hypothesis, which assumes that another parameter called turbulent viscosity or eddy viscosity is isotropic. The turbulence model used in this simulation is based on this hypothesis and calculates this eddy viscosity using an additional four transport equations. Flow variables in the following governing equations are written as averaged quantities in RANS equations. For convenience, these governing equations (Fluent 6.2 User's Guide) are written in symbolic notation. The equations in cylindrical coordinates, and the other two common sets of coordinates, can be easily converted by standard differential operations (Bird et al., 2002).

Continuity equation:

$$\frac{\partial \rho}{\partial t} + \nabla \cdot (\rho \vec{v}) = 0$$

Momentum equation:

$$\frac{\partial}{\partial t}(\rho \vec{v}) + \nabla \cdot (\rho \vec{v} \vec{v}) = -\nabla p + \nabla \cdot (\bar{\bar{\tau}} + \bar{\bar{\tau}}_t)$$

$$\bar{\bar{\tau}} = \mu \left[(\nabla \vec{v} + \nabla \vec{v}^T) - \frac{2}{3} \nabla \cdot \vec{v} \bar{\bar{I}} \right]$$

$$\bar{\bar{\tau}}_t = \mu_t \left[(\nabla \vec{v} + \nabla \vec{v}^T) - \frac{2}{3} \left(\frac{\rho k}{\mu_t} + \nabla \cdot \vec{v} \right) \bar{\bar{I}} \right]$$

Energy equation:

$$\frac{\partial}{\partial t}(\rho E) + \nabla \cdot (\vec{v}(\rho E + p)) = \nabla \cdot (k_{eff} \nabla T)$$

$$E = h - \frac{p}{\rho} + \frac{\upsilon^2}{2}$$

$$h = \int_{T_{ref}}^{T} c_p dT$$

$$k_{eff} = k + \frac{c_p \mu_t}{\mathrm{Pr}_t}$$

where T_{ref} = 298.15 K and Pr_t = 0.85.

The eddy viscosity (μ_t) in the Reynolds stress tensor term ($\overline{\overline{\tau}}_t$) and in the effective thermal conductivity (k_{eff}) is calculated using the turbulence model described in the following section.

Three fluid properties, i.e., dynamic viscosity (μ), specific heat (c_p), and thermal conductivity (k), are expressed by temperature-dependent functions, which are piecewise polynomials in three temperature ranges. These functions are added to the material database of FLUENT. The values of these properties are taken from the table of air properties at atmospheric pressure in Incropera & DeWitt (2002). As for the density of air, two functions are used in this thesis. The first one, used for the first two simulation cases, is the equation of state for ideal gases. With this function, the pulsating flows behave as a fully compressible flow because the density depends on both temperature and pressure.

Equation of state for ideal gases:

$$\rho = \frac{p}{RT}$$

$$R = \frac{\overline{R}}{MW}$$

The other function for density is a temperature-dependent piecewise polynomial function with the values taken from the same table as the other properties. This function, used in the third simulation case, is equivalent to the ideal gas law with constant pressure set to atmospheric pressure.

Turbulence Model

FLUENT provides several turbulence models, depending on the complexity of flow problems, ranging from a simple one-equation model to a sophisticated LES model. The common turbulence models for most flows are two-equation models, i.e., k-ε and k-ω families. The parameters in these models are calibrated with simple flows to mildly complex flows. In cases of complex and strongly separated flows, an appropriate choice is the υ^2-f or V2F turbulence model developed by Durbin (1991). This model solves four transport equations of turbulence parameters, two from the standard k-ε model (turbulence kinetic energy and dissipation rate, respectively) and another two for a velocity variance scale (υ^2) and an elliptic relaxation function (f). The latter two parameters were developed originally as a near-wall treatment for mildly separated flows. Nevertheless, it has been shown that this model is accurate for more complex flows and heat transfer, e.g., strongly separated flows (Durbin, 1995), unconfined and confined jet impingement heat transfer (Behnia et al., 1998, Behnia et al., 1999), pulsating channel flows (Scotti & Piomelli, 2002), and three-dimensional flows and heat transfer (Parneix et al, 1998, Etemad & Sundén, 2006). There are two reasons for selecting the V2F model for the simulation in this thesis. First, flow separation is expected to occur in pulsating flows at the tailpipe exit during flow reversal (from the observation of simulation results used for Liewkongsataporn et al., 2006a). Second, this model is also an excellent

candidate for simulating jet impingement heat transfer (Zuckerman & Lior, 2005) which is a main part in the PAD project.

The following equations are the V2F model in FLUENT (FLUENT 6.1 υ^2-f Turbulence Model Manual). Note that most symbols used in this model are designated differently from List of Symbols except for some common symbols, i.e., density (ρ), time (t), dynamic and kinematic viscosities (μ & ν), and velocity vector ($\vec{\upsilon}$).

$$\frac{\partial}{\partial t}(\rho k)+\nabla\cdot(\rho k\vec{\upsilon})=\overline{P}-\rho\varepsilon+\nabla\cdot\left[\left(\mu+\frac{\mu_t}{\sigma_k}\right)\nabla k\right]$$

$$\frac{\partial}{\partial t}(\rho\varepsilon)+\nabla\cdot(\rho\varepsilon\vec{\upsilon})=\frac{C'_{\varepsilon 1}\overline{P}-C_{\varepsilon 2}\rho\varepsilon}{\overline{T}}+\nabla\cdot\left[\left(\mu+\frac{\mu_t}{\sigma_\varepsilon}\right)\nabla\varepsilon\right]$$

$$\frac{\partial}{\partial t}\left(\rho\overline{\upsilon^2}\right)+\nabla\cdot\left(\rho\overline{\upsilon^2}\vec{\upsilon}\right)=\rho kf-6\rho\overline{\upsilon^2}\frac{\varepsilon}{k}+\nabla\cdot\left[\left(\mu+\frac{\mu_t}{\sigma_k}\right)\nabla\overline{\upsilon^2}\right]$$

$$f-L^2\nabla^2 f=(C_1-1)\frac{\frac{2}{3}-\overline{\upsilon^2}/k}{\overline{T}}+C_2\frac{\overline{P}}{\rho k}+\frac{5\overline{\upsilon^2}/k}{\overline{T}}$$

$$\overline{P}=2\mu_t S^2$$

$$S^2=\overline{\overline{S}}:\overline{\overline{S}}$$

$$\overline{\overline{S}}=\frac{1}{2}\left(\nabla\vec{\upsilon}+\nabla\vec{\upsilon}^T\right)$$

$$T'=\max\left[\frac{k}{\varepsilon},6\sqrt{\frac{\nu}{\varepsilon}}\right]$$

$$\overline{T}=\min\left[T',\frac{\alpha}{\sqrt{3}}\frac{k^{3/2}}{\overline{\upsilon^2}C_\mu\sqrt{2S^2}}\right]$$

$$L' = \min\left[\frac{k^{3/2}}{\varepsilon}, \frac{1}{\sqrt{3}}\frac{k^{3/2}}{\overline{\upsilon^2} C_\mu \sqrt{2S^2}}\right]$$

$$L = C_L \max\left[L', C_\eta\left(\frac{\nu^3}{\varepsilon}\right)^{1/4}\right]$$

$$\mu_t = \rho C_\mu \overline{\upsilon^2}\,\overline{T}$$

$$\alpha = 0.6,\ C_1 = 1.4,\ C_2 = 0.3,\ C_{\varepsilon 1} = 1.4,\ C_{\varepsilon 2} = 1.9,\ C_\eta = 70,\ C_\mu = 0.22,\ C_L = 0.23,$$

$$\sigma_k = 1,\ \sigma_\varepsilon = 1.3,\ C'_{\varepsilon 1} = C_{\varepsilon 1}\left(1 + 0.045\sqrt{k/\overline{\upsilon^2}}\right)$$

Computational Domain

An objective of this project is to simulate pulsating flows in the tailpipe of a Helmholtz pulse combustor. The simulation is intended to model the whole tailpipe so that flow characteristics along the tailpipe can be found. Therefore, in order to obtain physically accurate solutions, the computational domain and boundary conditions have to be reasonable for the tailpipe zone. In a Helmholtz pulse combustor, the pressure oscillation in the combustion chamber could be assumed spatially uniform due to relatively large volume and diameter compared to the tailpipe. Therefore, as FLUENT provides a "pressure-inlet" condition for a boundary condition, the computational domain could begin right at the entrance of the tailpipe. With this condition, the velocity profile at the tailpipe entrance would be relatively flat. At the exit of the tailpipe, although the pressure could also be assumed uniform and constant at atmospheric pressure, the velocity profile during flow reversal is not flat, but rather a line sink flow (Keller et al., 1993). Therefore, the end of the computational domain has to extend beyond the tailpipe exit. Moreover, because an experimental variable in this thesis is the ambient

temperature, the area after the tailpipe exit must be large enough such that the boundary conditions at the end of the computational domain do not significantly affect the flow at the tailpipe exit. Therefore, the computational domain consists of two parts: the tailpipe itself and a large space extending beyond the tailpipe exit as shown in Figure 3.1. In this domain, the volume after the tailpipe exit could be viewed as a decoupling tank used in the experiments at Sandia National Laboratories or as a large impingement zone for pulsating jets. As exiting jets propagate downstream impinging onto the bottom wall, the flows become wall jets traveling along the wall to the "outlet" side. Hence, at the "outlet" boundary, a major part of the flow is expected to be flow back into the domain bringing in the ambient air with a specified temperature. The "inlet" and "outlet" terms are used in the sense of the mean mass flow rate with respect to the computational domain because the fluid could flow in or out at these boundaries during the flow oscillation.

In order to simplify the simulation to be only two-dimensional, a circular cross-sectional tailpipe is used and the pulsating flows are assumed to be axisymmetric without swirl or rotation. The diameter of the tailpipe is determined such that the cross-sectional area is close to that of the square tailpipe in the reference.

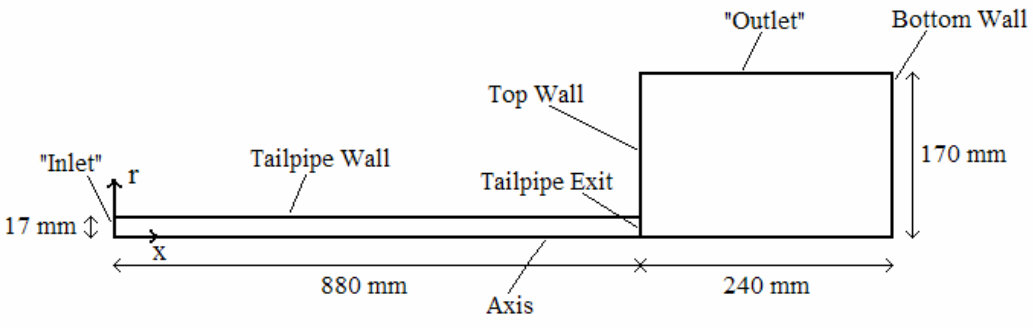

Figure 3.1: Computational domain

Grid Generation

Three sets of grid are used in this thesis. Grid 1, as a coarser grid, is used for preliminary simulation. As the computation domain is simple, a structured grid with rectangular cells is used. The domain in Grid 1 is divided into five zones, as shown in Figure 3.2, for the convenience of grid generation in each zone. First, nonuniform or geometric grid nodes are applied at the edges of each zone. Then the software GAMBIT automatically generates grid cells corresponding to the grid nodes. The arrows on the edges in Figure 3.2 indicate the direction of the nonuniform grid nodes, i.e., from finer grid to coarser grid. Table 3.1 shows the number of grid cells in each direction of each zone of Grid 1. The ratio in the rightmost column, commonly used for nonuniform grid, is the ratio between the sizes of adjacent cells.

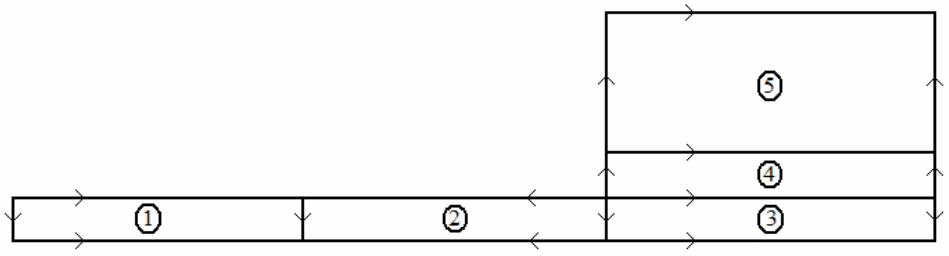

Figure 3.2: Diagram for the generation of Grid 1

Table 3.1: Number of grid cells for preliminary study (Grid 1)

Zone	Direction	No. of Cells	Ratio
1, 2	Axial	90	1.045
1, 2, 3, 4	Radial	40	1.03
3, 4, 5	Axial	70	1.05
5	Radial	40	1.06

For final results and grid independence study, Grids 2 and 3 are used. The computational domain is divided into eight zones as shown in Figure 3.3. Three zones are added from Grid 1 so that finer grid cells can be generated near the bottom wall. The number of cells and the ratios of each zone in Grids 2 and 3 are shown in Table 3.2.

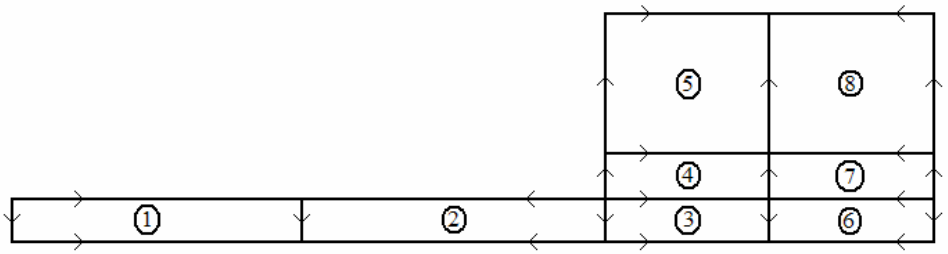

Figure 3.3: Diagram for the generation of Grids 2 and 3

Table 3.2: Number of grid cells for independence study (Grids 2 & 3)

Zone	Direction	No. of Cells	Ratio
1, 2	Axial	120 & 150	1.045 & 1.04
1, 2, 3, 4, 6, 7	Radial	60 & 80	1.03 & 1.03
3, 4, 5	Axial	70 & 100	1.06 & 1.05
6, 7, 8	Axial	50 & 70	1.06 & 1.05
5, 8	Radial	45 & 45	1.06 & 1.06

Note that the size of the smallest cells and the largest cells in either direction of each zone can be calculated from the length and the ratio in that direction, i.e.,

$$h_{\min} = L\left[\frac{R-1}{R^N-1}\right] \quad \text{and} \quad h_{\max} = h_{\min} R^{N-1},$$

where h is the cell size, L is the zone length in a particular direction, and R is the ratio of nonuniform grid.

Boundary Conditions

At the entrance of the tailpipe, or the "inlet" of the computation domain, the pressure-inlet condition is selected because this is close to an actual condition in the Helmholtz pulse combustor. Moreover, experimental data of pressure amplitude are available. An alternative condition for the simulation, mass-flow-inlet condition, could be applied if the amplitude of the mass flow rate oscillation is given. In FLUENT, the number specified in the pressure-inlet condition is taken as a total pressure for the simulation. At first, this seemed to be a problem because the experimental data were static pressure. Fortunately, the oscillation of pressure and velocity has a phase shift at a quarter of a cycle. Furthermore, the magnitude of dynamic pressure is typically much less than the magnitude of static pressure. Therefore, the total pressure oscillation and the static pressure oscillation are not considerably different. In fact, in FLUENT, when the velocity at the inlet is negative, i.e., out of domain, the dynamic pressure is set to zero, and the total pressure and the static pressure are the same. From the observation of preliminary results, the amplitudes of the oscillation of total and static pressure at the inlet are close. Only the mean values are different. Therefore, for the simulation in this thesis, the inlet boundary condition is total pressure oscillation with the amplitude from the reference, i.e., 10465 Pa.

The mean value of the inlet pressure oscillation is adjusted such that the time-averaged mass flow rate is close to a target value, 4 g/s. Because the adjustment of the value of the mean pressure is initially based on trial and error, preliminary simulation with Grid 1 was run several times, each time with a new mean pressure, until the target of

the mean mass flow rate was met. The final value served as the initial run for the simulation with Grids 2 and 3.

As shown in Figure 2.3, the pressure oscillation in the combustion chamber could be assumed sinusoidal. Therefore, the total pressure inlet condition is simply a mean value plus an oscillating part with a *sine* function:

$$p_t(t) = p_{tm} + p_{tA}\sin(\omega t)\,.$$

With this condition, the initial condition for the unsteady flow is a steady flow with a mean pressure value (p_{tm}) at the inlet. An inconvenience with this boundary condition, however, is that the steady flow for the initial condition has to be re-simulated every time the inlet mean pressure is changed. The oscillation frequency in the reference is 83 Hz. In the simulation, the frequency is set to be 83.33 Hz so that the period of the cycle is a whole number in millisecond units, i.e., 12 ms.

The temperature at the "inlet" is set to be uniform at 1500 K. This value is only for the flow entering the domain. When the flow is reversed, the "inlet" becomes an outlet of the domain, and the temperature at the "inlet" is determined by upstream flow from inside the tailpipe. The outlet condition for the energy equation is handled internally by FLUENT, which imposes a zero temperature gradient or zero heat flux at any outlet boundary. With these conditions, the temperature of fluid particles or cells at the "inlet" will experience a jump or non-continuous change when the cell velocity changes direction, especially from negative back to positive. However, this sudden change is not expected to affect the flow characteristics because the temperature oscillation at the entrance of the tailpipe is expected to be small. In fact, in an actual Helmholtz pulse

combustor, the temperature might indeed "jump" when the fresh hot flue gas is coming out of the combustion chamber.

The boundary conditions for the momentum equations at the walls are the no-slip condition. For the boundary conditions of the energy equation at the tailpipe wall, the temperature is assumed to be uniform and constant because no details were given in the reference. Because counter-flowing cooling air was used as a heat exchanger around the tailpipe, wall temperature was not expected to be uniform in the experiments. However, no information of temperature or heat flux was available except for one figure in the reference that showed temperature profiles at the base location. In that figure, the wall temperature was approximately 500 K. Therefore, for simplification, the tailpipe wall temperature for the simulation is set to be spatially uniform and constant at 500 K. At the other two walls, the top and bottom walls of the large impingement zone after the tailpipe exit, the boundary conditions for the energy equation are zero heat flux.

At the "outlet" of the computational domain, the boundary condition for the momentum equations is constant atmospheric pressure. As with the condition at the "inlet" or any boundary, FLUENT automatically assumes zero temperature gradient when the flow is out of the domain. At any outlet boundary of the domain, FLUENT also requires information for backflow temperature, which is technically an inlet condition when flow is reversed or enters the domain. The backflow temperature in this simulation is regarded as the ambient temperature. The values of this parameter are 850 K for Cases 1 and 3, and 300 K for Case 2. (Cases 1 and 2 are with the ideal-gas-law density function whereas Case 3 is with a temperature-dependent density function.) The ambient temperature for Case 1 is set to be higher than the temperature at the tailpipe exit in

Figure 2.10, which is about 700 K, so that the ambient temperatures for Cases 1 and 2 are greatly different.

Turbulence quantities

FLUENT provides several options to determine boundary conditions of turbulence parameters at inlet and outlet boundaries of the computational domain. In this simulation, the parameters are turbulence intensity (I) and hydraulic diameter (D_H). At the outlet boundary, these parameters are also required for backflow. For all study cases, the "inlet" boundary conditions are 10% for the turbulence intensity and 34 mm for the hydraulic diameter. These values are recommended by the FLUENT User's Guide for highly-turbulent and fully-developed internal flows. As for the ambient air, the turbulence level is assumed to be very low. Therefore, the "outlet'' boundary conditions are set to be 0.1% for the turbulence intensity and 1 mm for the hydraulic diameter, for all cases.

With these parameters, FLUENT automatically calculates other turbulence quantities at inlet boundaries, i.e., where flow enters the domain, as follows:

Turbulence length scale: $\ell = 0.07 D_H$

Turbulent kinetic energy: $k = \frac{3}{2}\left(u_{avg} I\right)^2$

Turbulent dissipation rate: $\varepsilon = C_\mu^{3/4} \frac{k^{3/2}}{\ell}$

Velocity variance scale: $\overline{\upsilon^2} = \frac{2}{3} k$

FLUENT also automatically assumes a zero-gradient condition at inlet boundaries for the elliptic relaxation function (f). At outlet boundaries where the flow is going out, FLUENT internally assumes zero-gradient for turbulence parameters. For boundary conditions at walls, FLUENT internally imposes values for turbulence parameters, which typically are zero for k and υ^2. As for the values for ε and f at walls, although the calculation is not given, it could be assumed that the following asymptotic solutions are used (Parneix et al., 1998):

$$\varepsilon_{wall} = 2\nu\left(\frac{k}{y^2}\right)_{wall} \quad \text{and} \quad f_{wall} = \frac{-20\nu^2}{\varepsilon}\left(\frac{\overline{\upsilon^2}}{y^4}\right)_{wall},$$

where y is the wall normal distance.

Numerical Schemes

For the preliminary simulation with Grid 1, the spatial discretization scheme is first-order upwind, and the temporal discretization scheme is first-order implicit. For the grid independence study with Grids 2 and 3 as well as for the simulation to obtain the final solutions, the second-order schemes are used in both space and time domain. For all simulation cases in this thesis, either steady or unsteady flows, the segregated solver is used. This solver in FLUENT sequentially solves the governing equations and iterates until the solutions converge, or until the iteration counter reaches a specified maximum value for steady flows, or in each physical time step for unsteady flows. The physical time step is 2.4 μs, i.e., 500 time steps in one oscillation cycle. And the maximum number of iterations allowed in each physical time step is 200. The pressure-velocity coupling method is SIMPLE for steady flows and PISO for unsteady flows. Other

parameters such as under-relaxation factors or constants in the turbulence model are default values.

Convergence criteria in FLUENT are based on the "scaled" residuals of conservation equations. An "unscaled" residual for each conservation equation is the summation of the imbalance of the discretized equation over all the computational cells. The scaled residual, except for the continuity equation, is the unscaled residual divided by a scaling factor which represents the flow rate of the main variable of the conservation equation through the domain. For the segregated solver, the scaled residual of the continuity equation is the unscaled residual divided by the largest absolute value of the unscaled residuals in the first five iterations. Unlike the residuals of the other conservation equations, the continuity residual largely depends on an initial condition. If the initial condition is good or close to the final condition, the continuity residual remains a relatively high value throughout the simulation. Therefore, the continuity residual is not used for the convergence criteria in this thesis. The convergence criteria of the scaled residuals for unsteady flows are 10^{-6} for the energy equation and 10^{-3} for the other equations. For steady flows used as initial conditions, the criteria of the scaled residuals are 10^{-7} for the energy equation, 10^{-5} for the momentum equations, and 10^{-4} for the turbulence transport equations.

CHAPTER 4

RESULTS AND DISCUSSION

There are three study or simulation cases in this thesis. Cases 1 and 2 are run with the ideal-gas-law density function. Case 3 is run with a temperature-dependent density function. The values of the ambient temperature or the backflow temperature at the "outlet" boundary are 850 K for Cases 1 and 3 and 300 K for Case 2. There are also three computational grids for each case. Grid 1 has a coarser grid with first-order discretization schemes for the preliminary study. Grids 2 and 3 have a greater total number of grid cells and finer grid cells at the walls with second-order discretization schemes for the final results and the grid independence study. Mean Reynolds numbers for flows with high and low ambient temperatures are about 3430 and 3770, respectively, whereas mean Womersley numbers are about 35 and 38, respectively, based on mean bulk velocity and temperature.

Preliminary Simulation Results

For comparison purpose, each study case of simulation had approximately the same mean mass flow rate. However, the setup of boundary conditions does not allow this value to be set directly. The parameter that indirectly determines this value is the mean inlet pressure, which has to be adjusted manually for each simulation run so that the mean mass flow rate matches the desired value. The process of finding the correct mean pressure is rather slow because it requires running the simulation several times. Furthermore, the simulation with each value of the mean pressure has to be run for

several cycles until the oscillation becomes relatively stable before the mean mass flow rate could be evaluated. The simulation with each mean pressure value also needs a different corresponding steady flow for an initial condition. Therefore, in order to speed up the process, Grid 1 was used to preliminarily find the mean pressure for each study case. Another purpose was to make certain that simulation solutions were physically reasonable before proceeding with Grids 2 and 3.

After several tries, mean pressure values of 700, 1450, and 500 Pa were selected which yielded mean mass flow rates of 4.3, 4.5, and 4.4 g/s, for Cases 1, 2, and 3, respectively. For the preliminary study, only axial velocity and temperature along the tailpipe center (axis) were monitored. Figure 4.1 shows time-averaged axial velocities for all three cases. The values for Cases 1 and 3 are roughly the same and similar to the experimental results in the reference (Figure 2.5). For Case 2, in which ambient temperature is much lower, the velocities near the exit are significantly lower than those in Case 1.

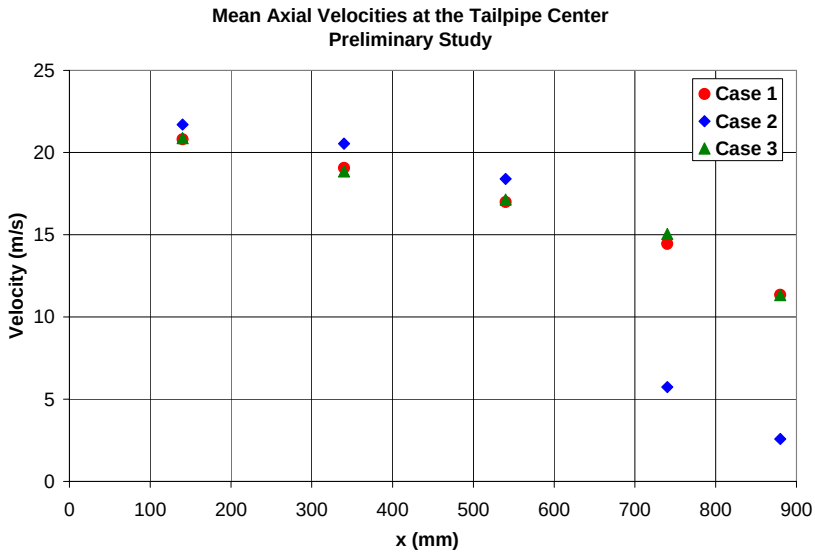

Figure 4.1: Mean axial velocities – all cases (Grid 1)

Figures 4.2 and 4.3 show the oscillating parts of the axial velocity at several axial positions for Cases 1 and 3, respectively. The pattern of oscillations in both cases could be assumed sinusoidal except for near the exit of the tailpipe. However, two major differences can be observed from these plots. In Case 1, the velocity amplitudes increase along the axis of the tailpipe and level off near the exit. In Case 3, the velocity amplitudes are similar everywhere except at the exit of the tailpipe. These two characteristics, from Cases 1 and 3, could be expected from compressible and incompressible flows, respectively. Although the density of fluid in Case 3 is not constant but varying with temperature, the results show an incompressible flow behavior, as expected. Furthermore, in Figure 2.5, another characteristic of velocity oscillation was a phase shift along the tailpipe. The oscillation was more symmetric near the exit than near the inlet. This characteristic could be seen in Figure 4.2, Case 1. On the other hand, the phase in Figure 4.3, Case 3, is approximately the same. At this point, it could be preliminarily concluded that pulsating flows in a pulse combustor tailpipe need to be treated as compressible flows, with the density variation effect from both pressure and temperature. As for the preliminary effects of the ambient temperature, the plots of axial velocity oscillation from Case 2 are shown in Figure 4.4. The pattern is no longer sinusoidal. The amplitudes are generally less than those in Case 1. Finally, the increase in amplitudes and the phase-shifted behavior along the tailpipe can still be observed.

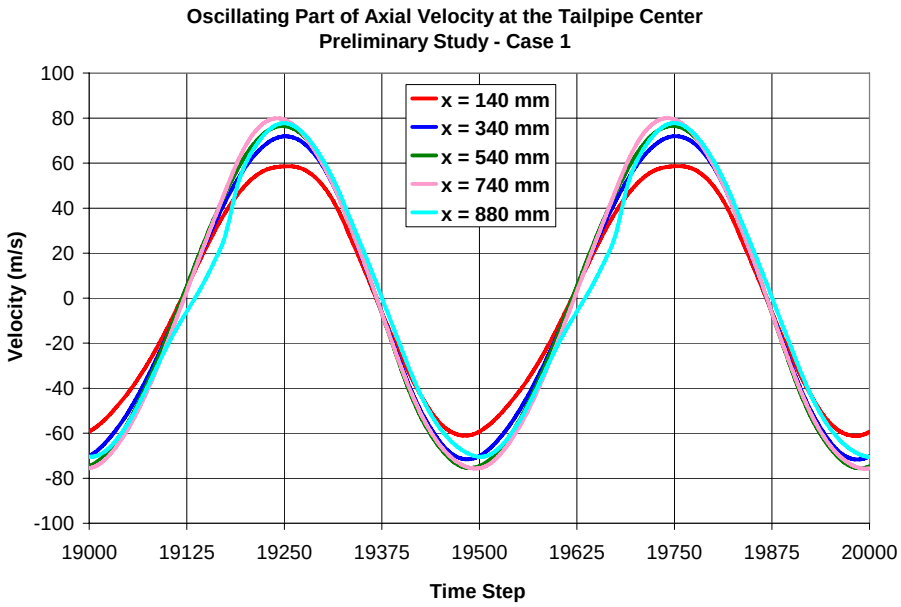

Figure 4.2: Oscillating part of axial velocity – Case 1 (Grid 1)

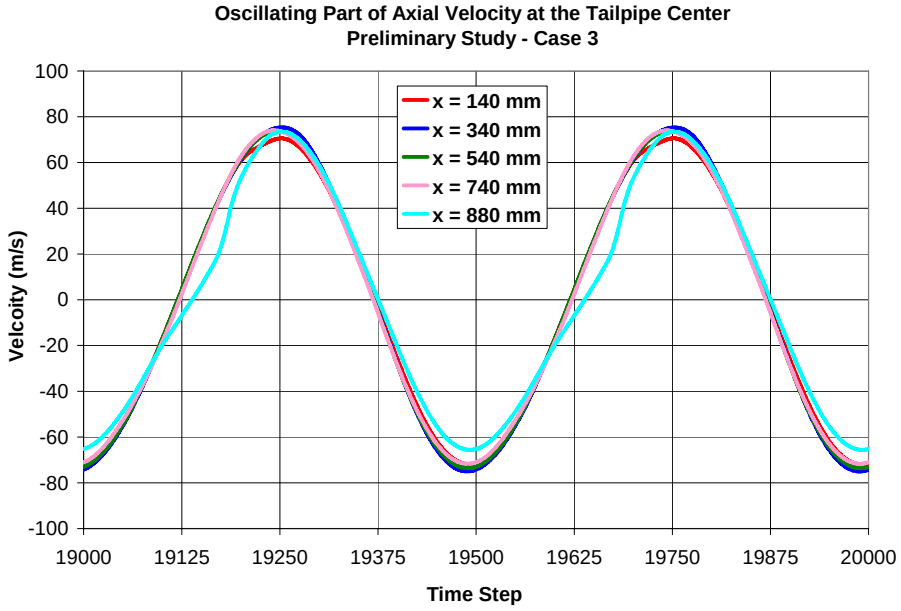

Figure 4.3: Oscillating part of axial velocity – Case 3 (Grid 1)

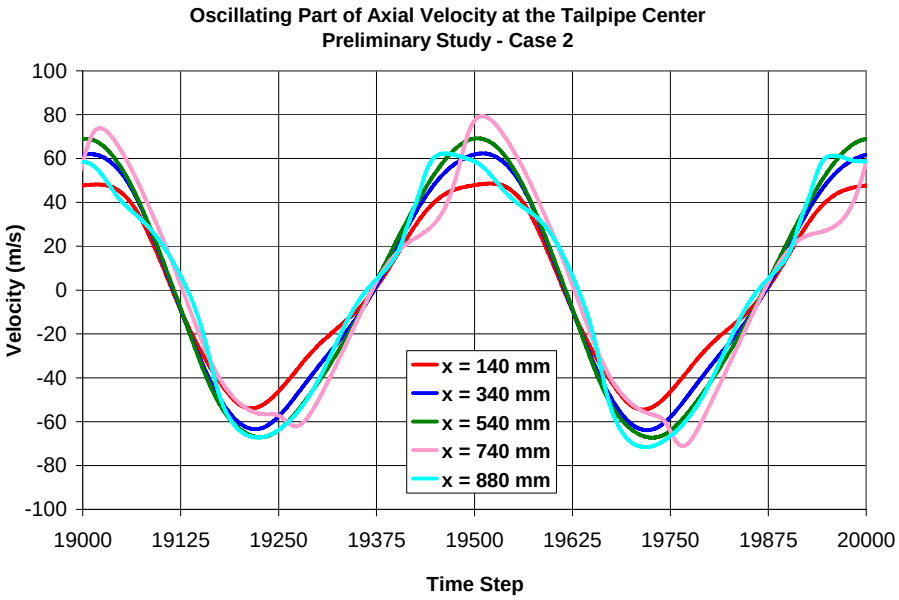

Figure 4.4: Oscillating part of axial velocity – Case 2 (Grid 1)

The values of the mean pressure of the inlet condition for three cases from this preliminary study would be used in the grid independence study as initial trials. From the plots of velocity oscillation along the tailpipe center, compared to the experimental results in the reference case, it seems that the simulation conditions and parameters in Case 1 were physically reasonable for these types of flows. Therefore, Case 1 would be used as a validation case for final results, and Case 2 would be used as a prediction case. Although the preliminary results from Case 3 seem physically inaccurate, this case would still be simulated in the grid independence study and for final solutions, for comparison with Case 1.

Grid Independence Study

As is common practice for CFD simulation, a grid independence study was performed. Final results reported in this thesis are from Grid 2, whereas Grid 3 is used for comparison in the grid independence study. At first, mean pressure values obtained from the preliminary study were used as initial values for Grid 2. Then, different values of mean pressure, based on initial solutions, were tried until the mean mass flow rates were close to the target. The final values of mean pressure were 725, 1365, and 520 Pa for Cases 1, 2, and 3, respectively. Unlike the results from Grid 1 where the oscillation of mean mass flow rates and velocities was very stable and repeatable after several cycles, the oscillation of mass flow rates and velocities from Grid 2 were never repeatable for consecutive cycles. Therefore, the mean mass flow rates were averaged from another 10 cycles after the oscillation became relatively stable, which took about 10 cycles. Thus, the total number of cycles for the simulation for the grid independence study was 20 cycles. The final values of mean mass flow rates were 4.04, 4.32, 4.06 g/s, for Cases 1, 2, and 3 respectively. For the grid independence study, the same values of mean pressure from Grid 2 were used with Grid 3. The result comparison was based on the oscillations of mass flow rate at the inlet and axial velocity at the axis and the same base location as in the reference (x = 540 mm).

For Case 1, Figures 4.5 and 4.6 show 10-cycle-averaged plots of inlet mass flow rate and axial velocity at the base location, respectively. Grid 3 yielded slightly greater values of mass flow rate and axial velocity than Grid 2. The difference for the mean mass flow rate and the mean axial velocity from Grid 3 with respect to Grid 2 is 18% and 12%, respectively. It could be assumed that if the mean pressure of Grid 3 was adjusted such

that the mean mass flow rate be equal to that of Grid 2, the difference for axial velocity would be lower. This difference in solutions between two grids is slightly too large for a typical grid independence study of steady flow simulation. However, considering the time spent for adjusting both the number of grid cells and the value of mean pressure for each set of grid, the difference of solutions between Grids 2 and 3 could be acceptable as a trade-off. Furthermore, the average computational time for Grid 3 was approximately double the time for Grid 2. Note that no attempt was made for further refining grid cells from Grid 3 because, from the observation during the simulation, the values of y^+ at the tailpipe wall for both Grids 2 and 3 were already less than 5. This value of y^+ is recommended by the FLUENT User's Guide for the simulation that needs to capture flow characteristics near a wall such as boundary layers or wall heat transfer.

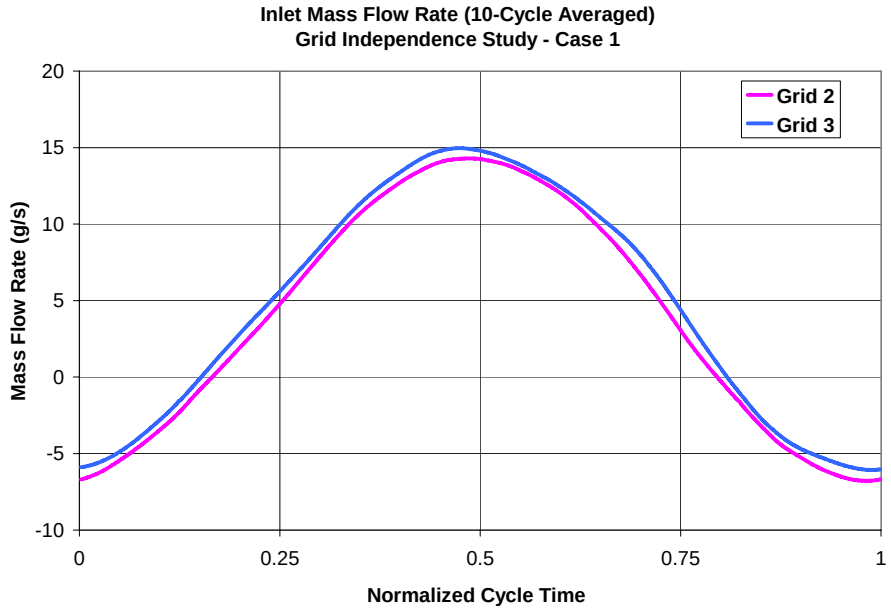

Figure 4.5: Inlet mass flow rate oscillation – Case 1 (Grids 2 & 3)

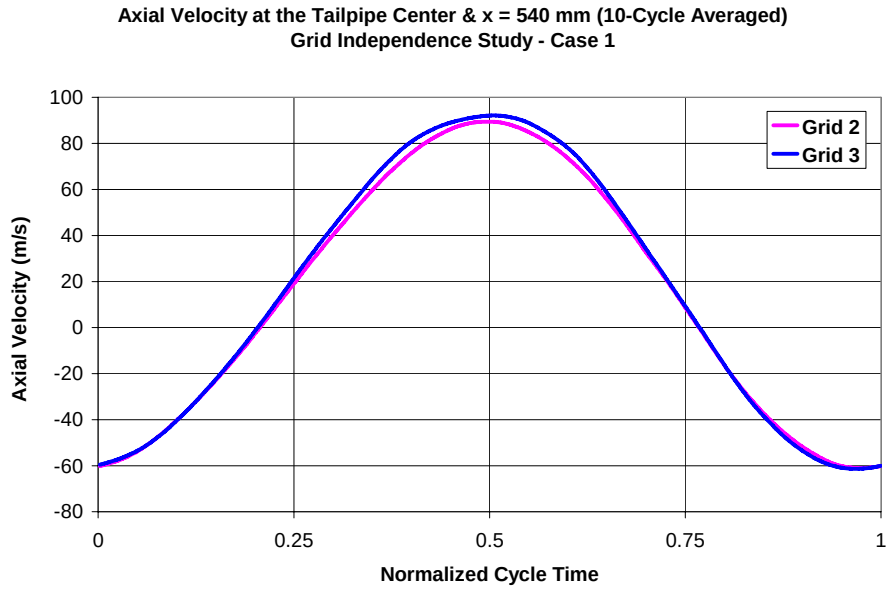

Figure 4.6: Axial velocity oscillation – Case 1 (Grids 2 & 3)

The same comparison was performed for Cases 2 and 3, and the results show a similar behavior to that in Case 1. The plots of mass flow rate and axial velocity for Cases 2 and 3 are shown in Figures 4.7 and 4.8 and, respectively. For Case 2, the differences for the mean mass flow rate and the mean axial velocity from Grid 3 with respect to Grid 2 were -8% and -11%, respectively. As with Case 1, these numbers were proportional. If the mean mass flow rate was adjusted to be the same between Grids 2 and 3, the difference in the mean axial velocity should be lower. However, for Case 3, the trend was opposite. That is the differences were 8% and -2% for the mean mass flow rate and the mean axial velocity, respectively. Nevertheless, as with Case 1, Grid 2 was used for the final solutions for Cases 2 and 3. Note that the phase difference in Figures 4.7 and 4.8 was because the negative sign was used in the equation of inlet pressure oscillation for Case 2, whereas the positive sign was used in Cases 1 and 3.

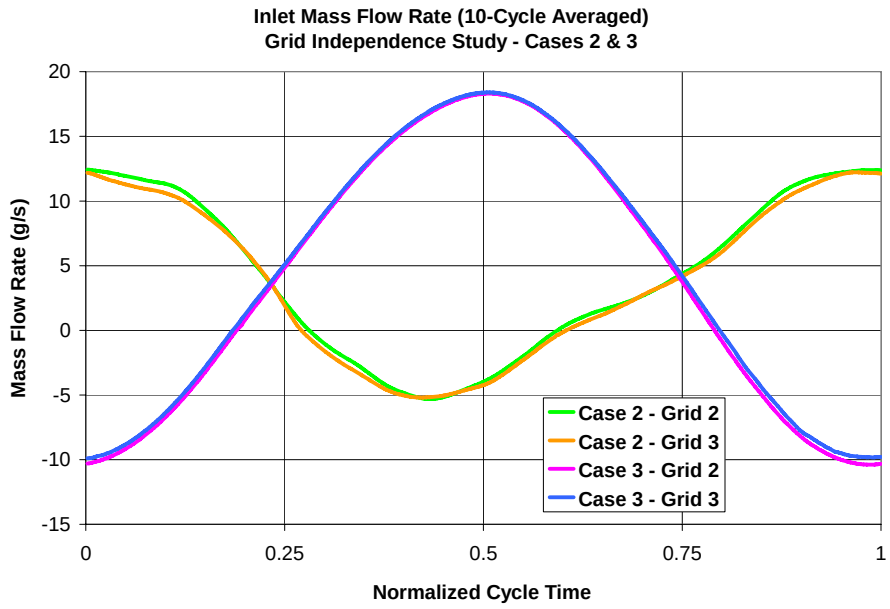

Figure 4.7: Inlet mass flow rate oscillation – Cases 2 & 3 (Grids 2 & 3)

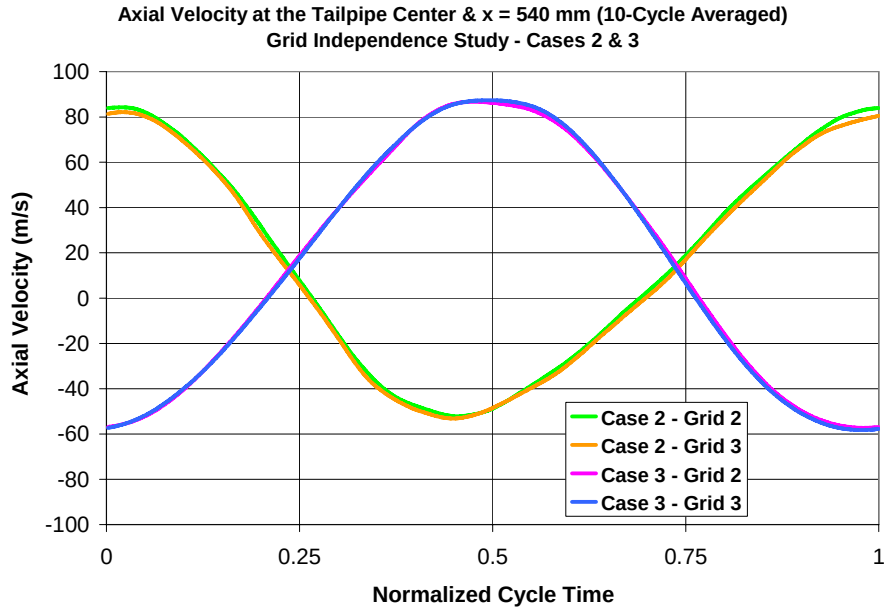

Figure 4.8: Axial velocity oscillation – Cases 2 & 3 (Grids 2 & 3)

Although Grid 2 was accepted for the final results of the simulation as the trade-off between the accuracy and the computational time, another approach was also tried for the grid independence study. This approach was to compare the results with steady flows at the maximum and minimum velocities of the oscillation. The flow at the maximum velocity corresponded to the temperature specified at the tailpipe entrance, whereas the flow at the minimum velocity corresponded to the ambient temperature. For the simulation of the maximum velocity flow of Case 1, the mass flow rate of 20 g/s was specified at the "inlet" boundary with the temperature of 1500 K. A steady solver in FLUENT was used for both Grids 2 and 3. Figure 4.9 show the plots of axial velocity along the tailpipe center for the steady flows with maximum velocities of Case 1. The difference between Grids 2 and 3 are essentially negligible for this particular flow.

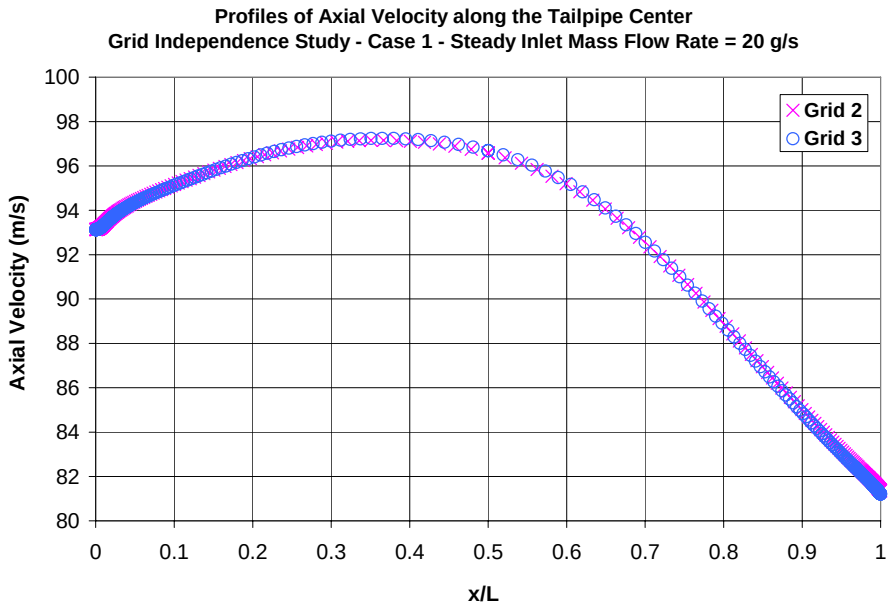

Figure 4.9: Velocity profiles along the axis – Case 1 at maximum velocity (Grids 2 & 3)

For the simulation of the minimum velocity flow of Case 1, the pressure-outlet condition was used as the boundary condition at the "inlet" boundary with a target of mass flow rate at -24 g/s. FLUENT automatically adjusted the pressure level at the "inlet" such that the target mass flow rate was met. The final value of the pressure was a vacuum pressure level because the pressure at the "outlet" was fixed at atmospheric pressure. The temperature of the flow in the computational domain corresponded to the temperature at the "outlet" boundary as an actual inlet in this particular flow. Initially, a steady solver was used for both Grids 2 and 3. Grid 2 yielded smooth convergence of the residuals, resulting in a steady flow solution. However, Grid 3 did not yield a steady flow solution. The plots of residuals were fluctuating, indicating an unsteady flow behavior. Therefore, an unsteady solver was used for Grid 3 for the simulation of this particular case. The physical time step was 24 μs. FLUENT automatically calculated the mean values of main flow variables when an unsteady solver was used. Thus, the solution from Grid 3 was able to be compared with the steady solution from Grid 2.

Figure 4.10 shows the plots of axial velocity along the tailpipe center for the flows with minimum velocity of Case 1. The results from Grid 3 were time-averaged values from unsteady solutions. Unlike the flow with maximum velocity, the two plots in Figure 4.10 look very different. From the observation of the solutions from both Grids, the difference in flow structure began at the tailpipe exit. In the case of Grid 2, there was a region of flow separation "bubble" or recirculating flow at the tailpipe wall beginning from the edge of the tailpipe exit. This flow characteristic is common for a flow past a blunt object. For Grid 2, the region of the recirculating flow was stable. However, for Grid 3, where the grid is finer near the wall than Grid 2, the recirculating flow was not

stable, but showed a behavior like a vortex-shedding flow originating from the edge of the tailpipe exit. Figure 4.11 shows an instantaneous contour of velocity magnitude for this particular flow from Grid 3. In fact, this behavior, vortex-shedding like, could also be observed in the solutions of the pulsating flow during the phase of flow reversal from Grid 3, but not from Grid 2. This behavior could be another reason for the difference between the results of Grids 2 and 3 in pulsating flows. As for Cases 2 and 3, the same approach of the simulation and comparison were performed. Similar results and behavior of maximum and minimum flows were obtained.

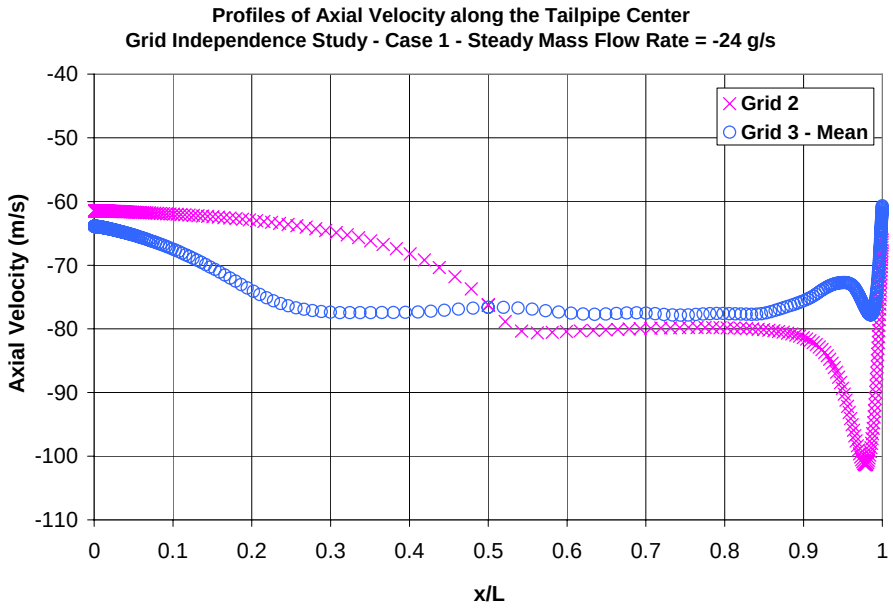

Figure 4.10: Velocity profiles along the axis – Case 1 at minimum velocity (Grids 2 & 3)

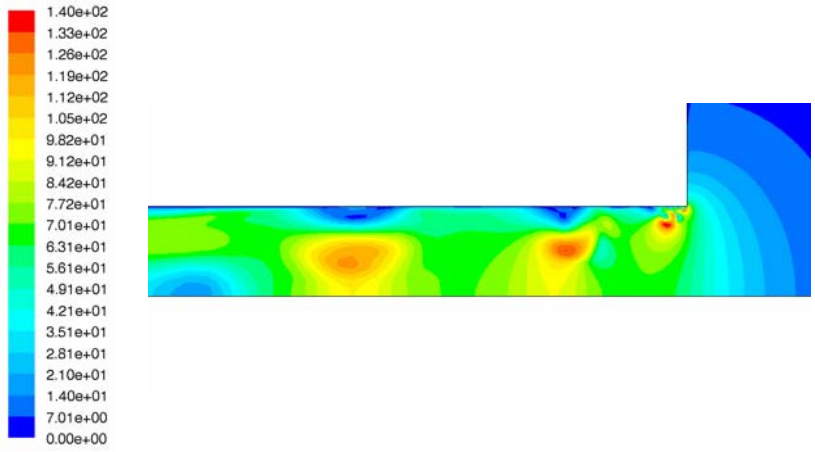

Figure 4.11: Contour of instantaneous velocity magnitude near the tailpipe exit – Case 1 at minimum velocity (Grid 3)

Initially, the unsteady behavior as shown in Figure 4.11 was taken as a physical characteristic of the flow. However, this behavior could also be a numerical characteristic of the simulation with the V2F model. According to Laurence et al. (2004), when the grid cells near walls are too small, typically $y^+ < 1$, there appear to be numerical stability problems with the V2F turbulence model in a segregated solver, which could lead to oscillation or divergence of the solution. From the observation of the simulation results in this particular flow, the values of y^+ in Grid 3 were indeed less than one at the wall near the tailpipe exit, whereas those in Grid 2 were in the range of 2-3. As for the case of the steady flow with the maximum mass flow rate, the values of y^+ in Grids 2 and 3 were greater than one everywhere along the tailpipe wall. Although these values of y^+ at the wall seem to support the idea of the numerical instability caused by the V2F model, detailed investigation of this unsteady behavior is recommended for future work because if this behavior is a physical flow characteristic, it might affect the characteristics of exiting jets and impingement heat transfer.

For the summary of the grid independence study, the solutions of pulsating flows from Grid 2 were slightly different from those from Grid 3 for all three cases, as shown in Figure 4.5-4.8. In another approach with steady maximum and minimum flows, the solutions were relatively the same between Grids 2 and 3 for the maximum flows of all cases. The major difference of the results was from the flows with minimum velocity and ambient temperature. The solutions from Grid 3 showed an unstable behavior like a vortex-shedding flow, whereas the solutions from Grid 2 were stable. The difference in similar behavior between Grids 2 and 3 was also observed in pulsating flows during flow reversal. At this point, it is not certain whether this behavior is a physical flow characteristic because it could also be a numerical characteristic caused by the instability problem of the turbulence model when the grid cells near the wall were too small. However, considering the computational time of the simulation with Grid 3, which was about twice that of Grid 2, and the results in Figures 4.5-4.8, Grid 2 was chosen for the simulation for the final results.

Final Simulation Results

All simulation results presented in this section were performed with Grid 2. The simulation was run for an additional 10 cycles beyond that used for the grid independence study so that more information on flow variables could be monitored and collected. For Case 1, as the validation case, representative results are compared with experimental results from the reference literature. A comparison between the three study cases focuses on the oscillation of bulk velocity and bulk temperature at various locations along the tailpipe.

Case 1: High Ambient Temperature

The time-averaged mass flow rate at the inlet of Case 1 over 10 cycles was 4.04 g/s. For a comparison with the experimental results in the reference, axial velocity oscillations at the same four positions and also at the inlet and the exit of the tailpipe are plotted in Figure 4.12. At the base location, x = 540 mm, the mean, maximum, and minimum velocities from the simulation were 14.3, 90, and -60 m/s, respectively, compared to 16.3, 95, and -60 m/s from the experiment. The numbers are in good agreement considering several different conditions such as the tailpipe shape, fluid properties, wall temperature, and ambient temperature. The values of mean velocities and oscillation amplitudes at all six locations are summarized in Table 4.1. The amplitude of the oscillations of flow variables in this thesis was simply calculated by (maximum value - minimum value)/2 because the pattern of most of the oscillations could be assumed sinusoidal.

The values in Table 4.1 are also in agreement with the experimental results (Figure 2.5). The mean velocities decrease but the amplitudes increase along the tailpipe. Figures 4.13 and 4.14 show instantaneous axial velocity profiles across the tailpipe at x = 540 mm during accelerating and decelerating phases, respectively. The profiles have no overshoot at maximum or minimum velocities, similar to the results in the reference. The unsteady part of the boundary layer is limited to within 2-3 mm from the wall, as in the experimental data in Figure 2.4.

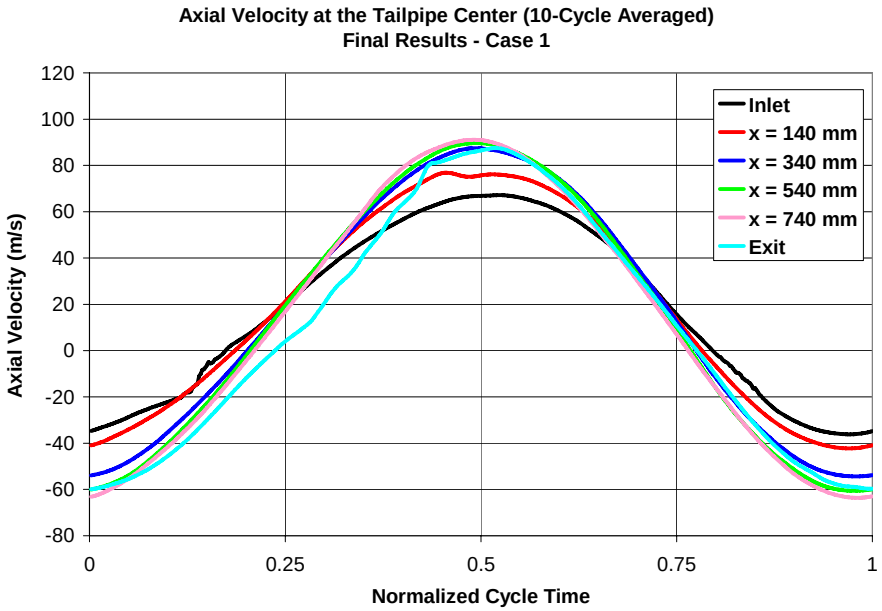

Figure 4.12: Axial velocity oscillation – Case 1

Table 4.1: Mean and amplitude of axial velocity (unit: m/s) at the tailpipe center – Case 1

Axial Position	Inlet	140 mm	340 mm	540 mm	740 mm	Exit
Mean	17.1	18.3	16.2	14.3	13.1	9.9
Amplitude	51.7	59.6	70.9	75.2	77.4	73.7

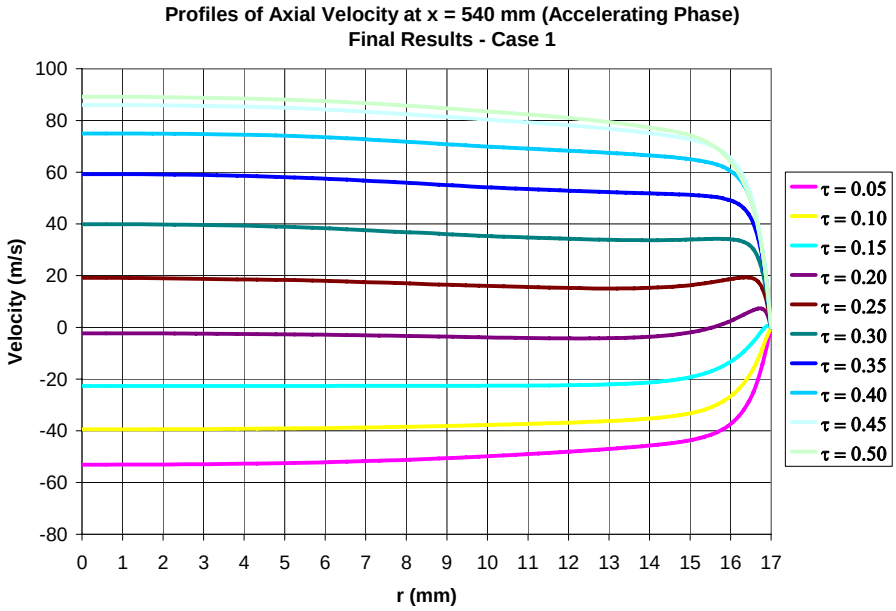

Figure 4.13: Axial velocity profiles (accelerating phase) – Case 1

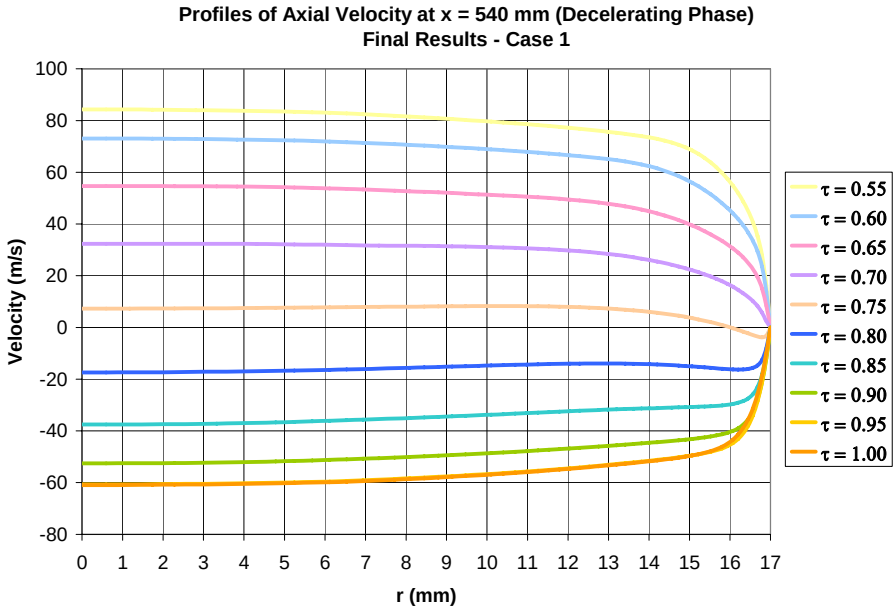

Figure 4.14: Axial velocity profiles (decelerating phase) – Case 1

Figure 4.15 shows the oscillation of temperature at the same six positions along the tailpipe center. The pattern of the temperature oscillation is different from the experiment (Figure 2.7) mainly due to the cross-section shape of the tailpipe. For the square tailpipe in the experiment, secondary flows produced when the flow was changing direction were expected to affect the heat flux and temperature. On the other hand, in this simulation, the pulsating flow was forced to be axisymmetric and, thus, had no secondary flows. However, simulation results could be compared with the first harmonic portion of experimental results (Figure 2.6). The temperature reaches a minimum value when the velocity is about to change from negative to positive. During the phase with negative flow velocity, the cooler fluid from the tailpipe exit side flows back to the position evaluated until the flow changes direction again. The opposite occurs when the velocity is positive until it is about to change to negative. The time-averaged temperature decreases along the tailpipe due to heat loss to the wall.

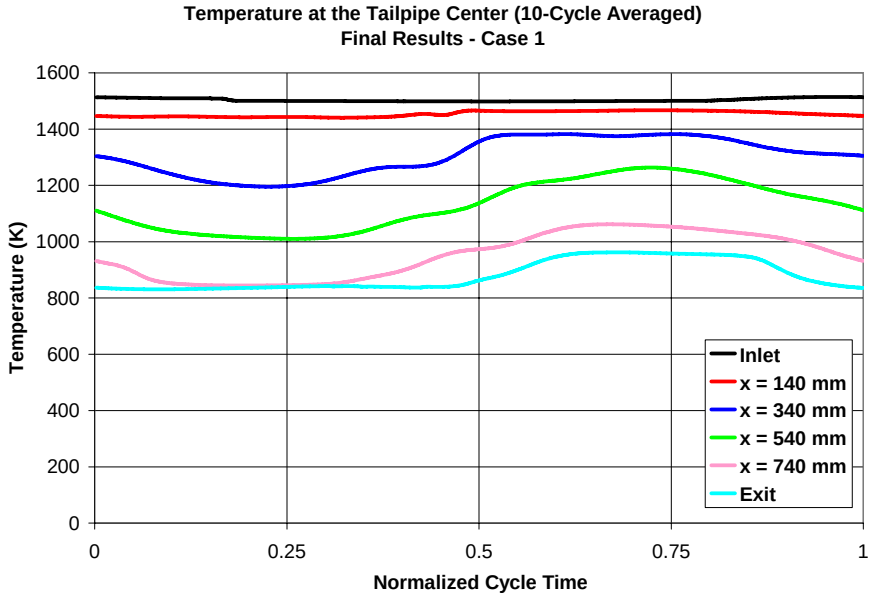

Figure 4.15: Temperature oscillation along the axis – Case 1

The simulation solutions of velocity and temperature oscillation at the center of the tailpipe confirm that the simulation conditions are comparable to the pulsating flow in a Helmholtz pulse combustor tailpipe. Next, for the comparison between cases, velocity and temperature oscillation of the bulk flow were considered. The bulk velocity is defined by

$$u_b = \frac{\int \rho u dA}{\int \rho dA}.$$

The bulk temperature in this thesis is a mass-flux-weighted averaged, defined by

$$T_b = \frac{\int T\rho|u|dA}{\int \rho|u|dA}.$$

Figure 4.16 shows the oscillation of bulk velocity at six positions along the tailpipe. Compared to the oscillation of velocity at the center of the tailpipe in Figure 4.12, bulk velocity oscillation shows more noticeable characteristics. The amplitude clearly increases with the axial distance. The phase shift is also more obvious. And the pattern of oscillation is smoother. The values of mean bulk velocity and corresponding amplitude are summarized in Table 4.2. As expected, the magnitude of velocity amplitude in Table 4.2 is less than that of velocity oscillation at the axis (Table 4.1).

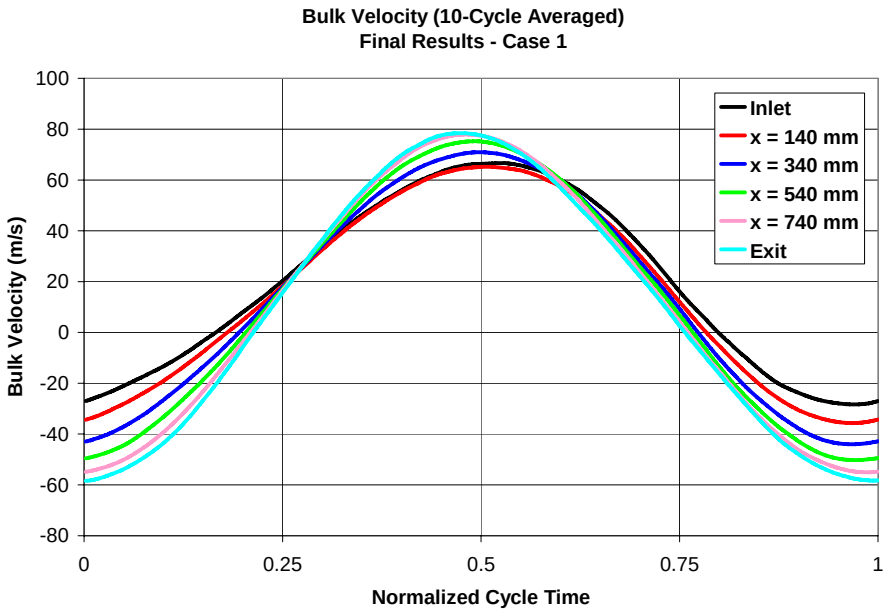

Figure 4.16: Bulk velocity oscillation – Case 1

Table 4.2: Mean and amplitude of bulk velocity (unit: m/s) – Case 1

Axial Position	Inlet	140 mm	340 mm	540 mm	740 mm	Exit
Mean	19.4	15.7	13.7	12.1	10.6	9.1
Amplitude	47.5	50.4	57.5	62.7	66.4	68.4

The oscillation of bulk temperature, as shown in Figure 4.17, appears to be significantly different from the temperature oscillation at the axis (Figure 4.15). There is a sudden drop in temperature when the bulk flow changes direction. This behavior is seemingly similar to the temperature oscillation in the square tailpipe. However, the reason is different for this simulation, i.e., the definition of bulk temperature by mass-flux-weight averaged. When the bulk velocity approaches zero, the profile of the velocity

across the tailpipe is not all zero. The fluid near the wall has phase-lead velocity, thus, greater magnitude than the fluid away from the wall. The temperature is lower near the wall than away from the wall. Thus, the density near the wall is higher. Mass fluxes near the wall at these moments are much greater than mass fluxes away from the wall. Therefore, the mass flux combined with lower temperature near the wall causes a sudden drop in bulk temperature at the point when bulk flow changes direction.

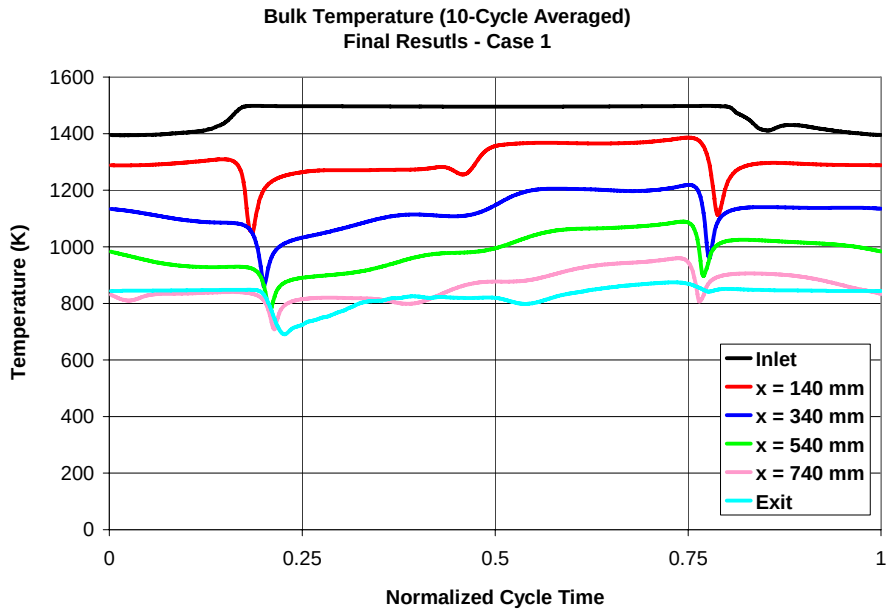

Figure 4.17: Bulk temperature oscillation – Case 1

Case 2: Low Ambient Temperature

Figure 4.18 shows the oscillation of bulk velocity of Case 2. Table 4.3 summarizes the mean values and the amplitude of bulk velocity oscillation. Compared to Case 1, the phase of oscillation is opposite because the equation of inlet pressure oscillation has the opposite sign. This was done so that the oscillation could reach

"steady-state" faster in this condition. As for the effect of cooler ambient temperature, the pattern of oscillation is irregularly sinusoidal at all locations except at the exit of the tailpipe. Another effect is that the amplitudes of oscillation are lower than those in Case 1. For the mean velocity, the values are generally greater than those in Case 1, due to the slightly greater mean mass flow rate as mentioned earlier (4.04 and 4.32 g/s for Cases 1 and 2, respectively).

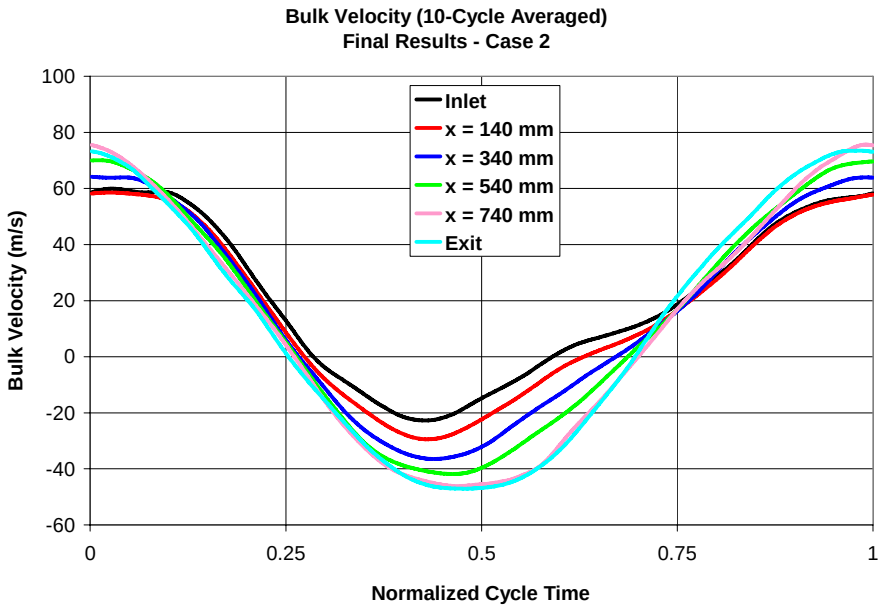

Figure 4.18: Bulk velocity oscillation – Case 2

Table 4.3: Mean and amplitude of bulk velocity (unit: m/s) – Case 2

Axial Position	Inlet	140 mm	340 mm	540 mm	740 mm	Exit
Mean	20.2	16.6	14.7	13.2	10.9	11.5
Amplitude	41.3	44.0	50.3	55.9	60.9	60.3

Figure 4.19 shows the oscillation of bulk temperature at various locations along the tailpipe. Compared to Figure 4.17 of Case 1, the pattern and the level of temperature are about the same from the inlet up to x = 540 mm. The pattern begins to differ at x = 740 mm, indicating the cooler ambient air reaches back up to at least this position. At the exit, the temperature level stays low at about ambient level (300 K) longer than half of the cycle. This confirms the behavior as explained by Keller et al. (1993) at the exit of the tailpipe (Figures 2.8 and 2.9). During flow reversal, fluid around the tailpipe exit is drawn into the tailpipe. When flow is reversed again, it takes some time to drive out that portion of fluid. Then, finally, fresh hot fluid from further inside the tailpipe is driven out of the tailpipe.

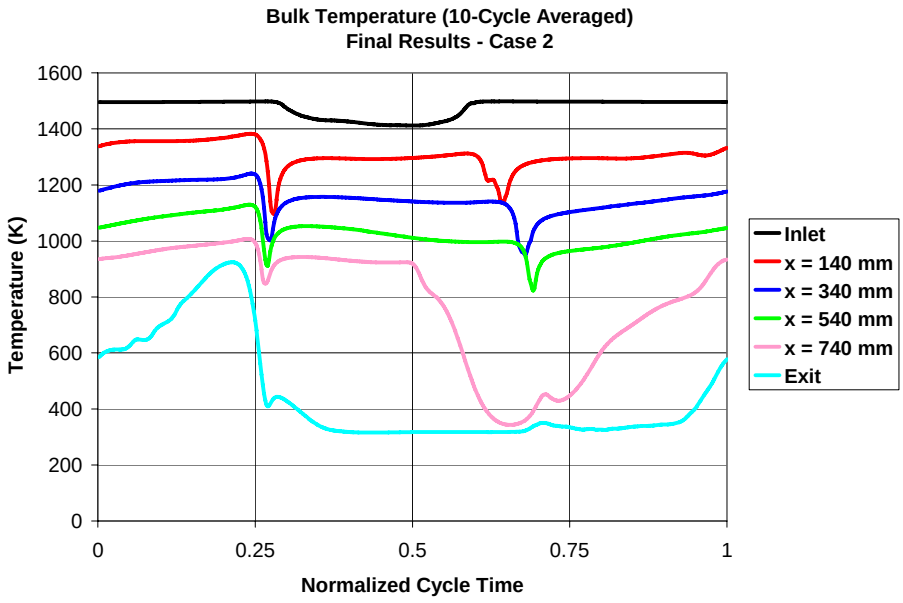

Figure 4.19: Bulk temperature oscillation – Case 2

In order to present a clearer visualization of pulsating flows near the tailpipe exit, contours of instantaneous temperature at various times in one cycle are shown in Figure 4.20. A similar behavior was also observed in Case 1. However, the color in the contours for Case 2 is more distinguishable due to larger difference in temperature inside and outside the tailpipe. Several characteristics can be observed from these contours. The reversed flow from outside the tailpipe is limited to some distance from the tailpipe exit. The temperature in the first half of the tailpipe (the entrance side) changes very little over the cycle. When the flow changes direction, fluid near the wall leads fluid near the axis. There is some instability in the exiting jet. This instability is in fact coherent structures or toroidal vortices, experimentally observed in Keller et al. (1993). Similar structures also occur in the simulation as shown in Figure 4.21, contours of instantaneous stream function. In each cycle, the vortices originate at the edge of the tailpipe exit when fluid near the wall begins to flow out of the tailpipe. Eibeck et al. (1993) showed by numerical simulation that toroidal vortices propagated downstream at a different speed, independently, from the exiting core jet and played a major role in impingement surface heat transfer enhancement. However, from the contour plots in Figures 4.20 and 4.21, the vortices and the core jet seem to propagate together. Note that the normalized cycle times in Figures 4.20 and 4.21 were shifted half a cycle with respect to the normalized cycle times in Figures 4.18 and 4.19. Therefore, the first contours in Figures 4.20 and 4.21 corresponded with the velocity close to the minimum velocity.

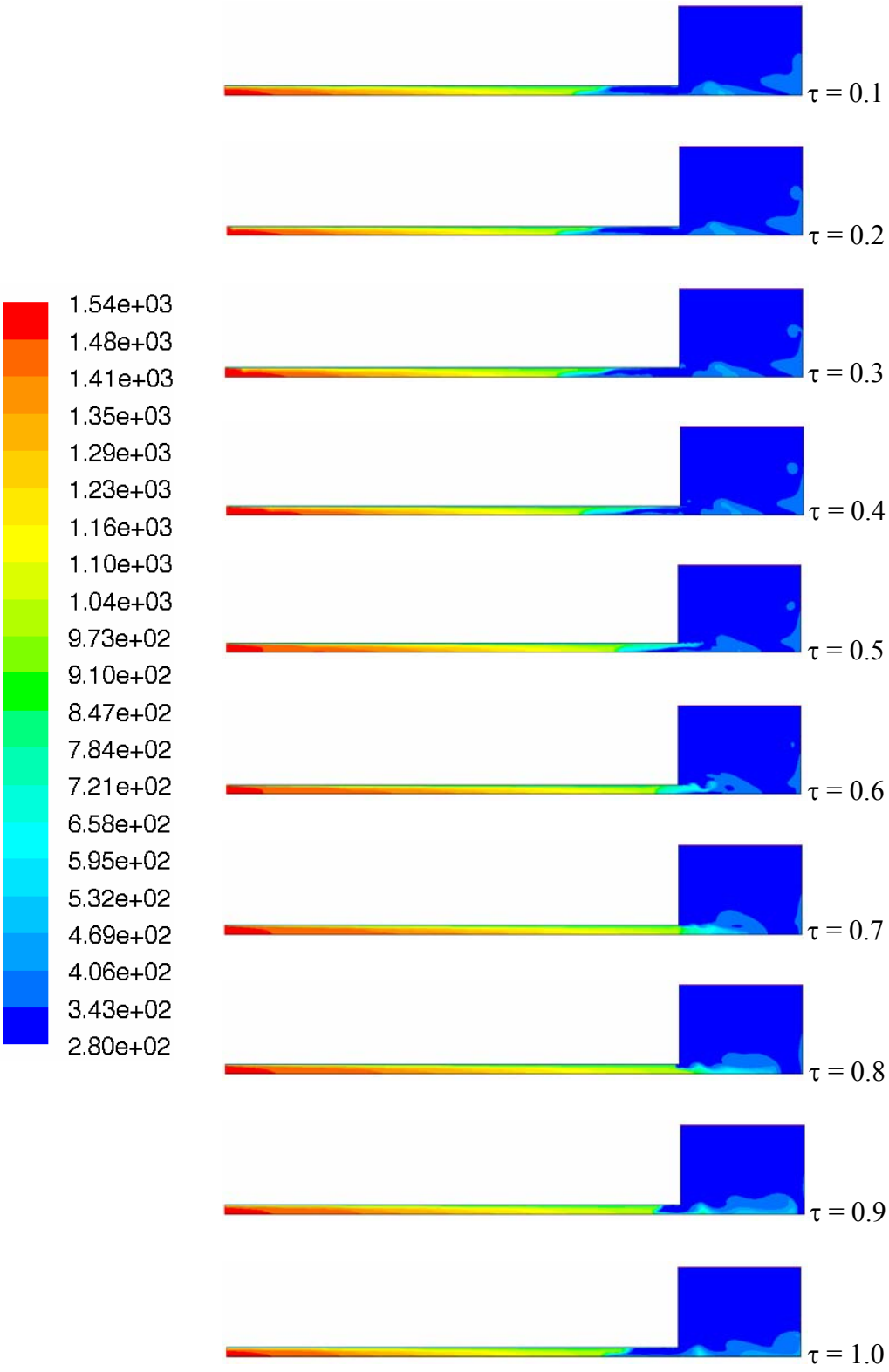

Figure 4.20: Contours of Instantaneous Temperature (unit: K) – Case 2

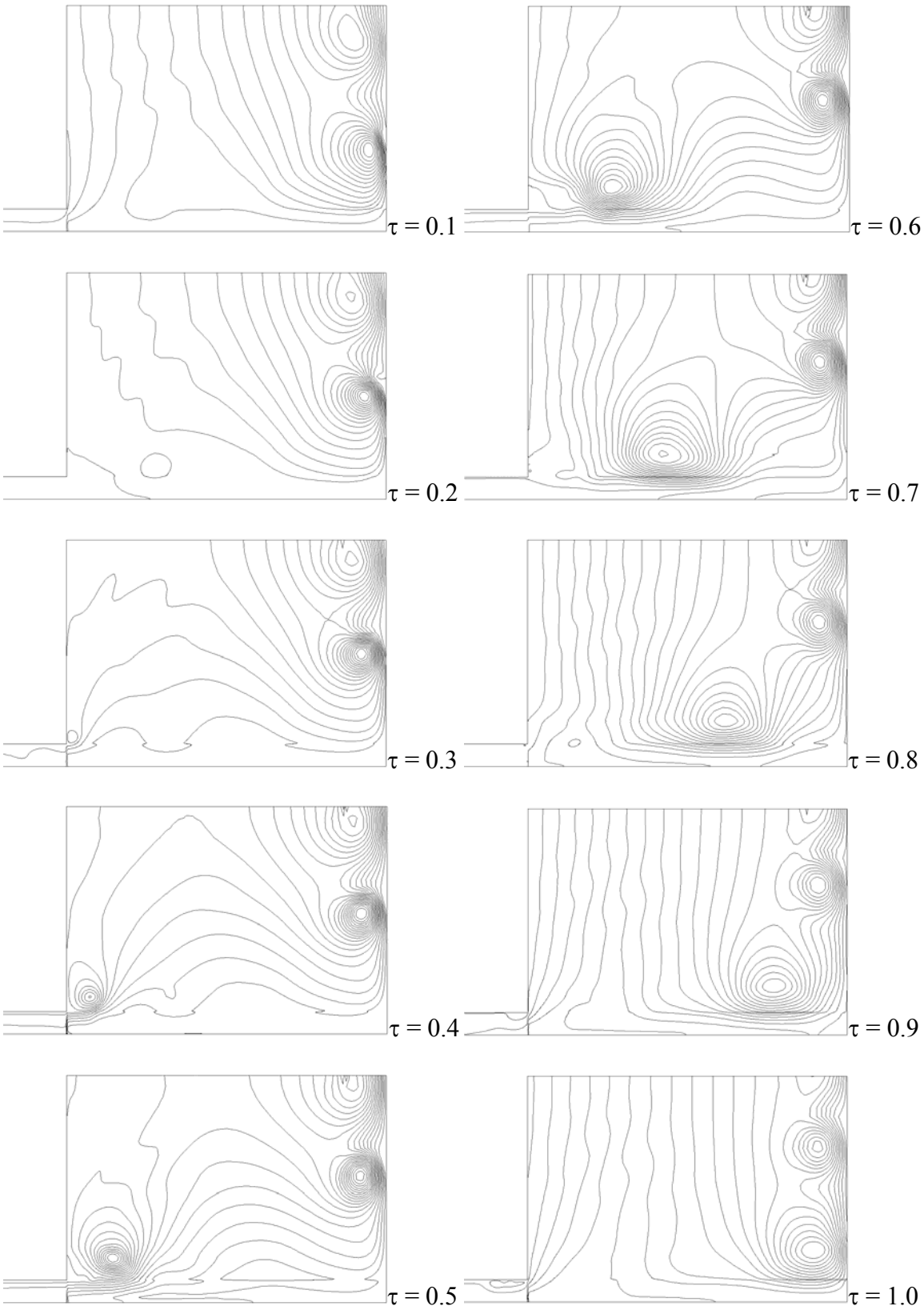

Figure 4.21: Contours of instantaneous stream function – Case 2

Case 3: High Ambient Temperature with a Temperature-Dependent Density Function

From the preliminary results, the pulsating flow with a temperature-dependent density function expectedly behaved like an incompressible flow. However, the results were based on axial velocity at the center of the tailpipe. The oscillation of bulk velocity would further confirm this characteristic. Figure 4.22 shows plots of bulk velocity oscillation along the tailpipe. Table 4.4 summarizes the mean and amplitude values of the oscillation of the bulk velocity. As with preliminary results, the amplitudes along the tailpipe are approximately the same everywhere.

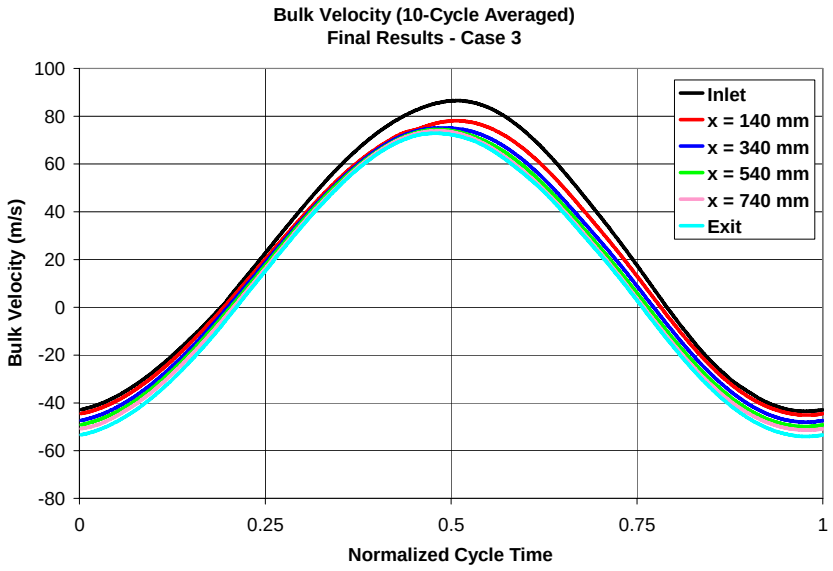

Figure 4.22: Bulk velocity oscillation – Case 3

Table 4.4: Mean and amplitude of bulk velocity (unit: m/s) – Case 3

Axial Position	Inlet	140 mm	340 mm	540 mm	740 mm	Exit
Mean	20.7	16.5	13.7	11.9	10.4	9.0
Amplitude	65.0	61.6	61.6	62.2	62.6	63.4

Another interesting characteristic in Case 3 is pressure oscillation inside the tailpipe. Although the pressure oscillation at the inlet is normally smooth, the pattern of pressure oscillation inside the tailpipe in Case 3 is not as smooth as that of Case 1, as shown in Figure 4.23. The pattern at other positions is also similar, although the mass balance in every computational grid cell was satisfied by the simulation. This is possibly because the density function used in Case 3 is not as physically accurate as the ideal-gas density function in Cases 1 and 2. This physical inaccuracy also caused the simulation to take much longer computational time for Case 3 than Case 1 because some residuals did not converge within a specified number of maximum iterations (200 iterations per time step). The averaged computational time for Case 3 was approximately four times of that for Case 1.

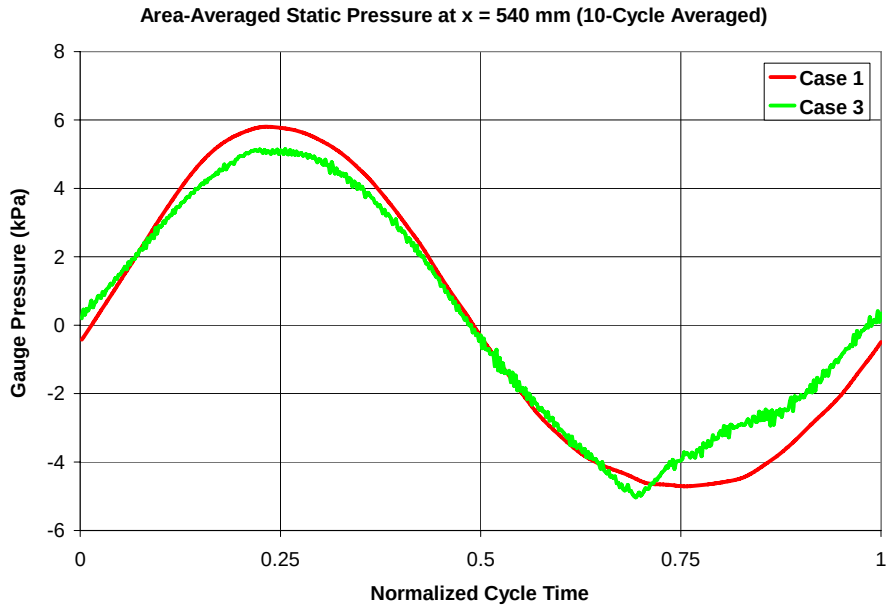

Figure 4.23: Pressure oscillation comparison between Cases 1 and 3

Summary of Final Results

The simulation results showed similar behaviors to the experimental data in the reference literature. The results confirmed that the pulsating flows in a pulse combustor tailpipe behaved more like compressible flows than incompressible flows. That is, the amplitude of velocity oscillation increased along the tailpipe. As for the effect of cooler ambient air on the temperature within the tailpipe, the results also confirmed that the effect was limited only to a short distance from the tailpipe exit. However, as an overall effect, the velocity amplitude along the tailpipe was lower than the case with higher ambient temperature. Finally, the simulation with a temperature-dependent density function was not physically accurate in terms of velocity and pressure oscillation. In the next section, data at a greater number of positions along the tailpipe were collected so that the profiles of flow variables could be more clearly observed and analyzed.

Comparison of Axial Profiles of Bulk Flow Variables

The simulation results in this section were obtained from two consecutive oscillation cycles in each case. These two cycles were chosen such that the time-averaged mass flow rate for each case was close to 4.0 g/s. The simulation was repeated to obtain bulk temperature, bulk velocity, and area-averaged static pressure at eleven positions from the inlet to the exit of the tailpipe. In addition, temperature and density within the tailpipe volume were also averaged and collected. The temperature was mass-flux-averaged, whereas the density was volume-averaged. The values of axial profiles in this section were averaged from the selected two oscillation cycles.

Figure 4.24 shows the profiles of time-averaged bulk temperatures along the tailpipe from all three cases. The effect of cooler ambient air is clearly shown in the

profile from Case 2. The temperatures at the exit for Cases 1, 2, and 3 were approximately 830, 445, and 820 K, respectively. As expected, the effect was limited only to a region near the exit. The cooler air in Case 2 traveled into the tailpipe approximately 180 mm. The profiles upstream before this point are approximately the same for all cases. The distance that ambient air could travel is directly related to the minimum velocity and the duration of the flow reversal. Since the oscillations are close to sinusoidal, it could be estimated by

$$L_{rev} = \frac{|u_{\min}|}{\sqrt{2}} \frac{T_{period}}{2}, \tag{4.1}$$

where L_{rev} is the distance that ambient air could travel, u_{min} is the minimum bulk velocity at the tailpipe exit, and T_{period} is the period of the oscillation cycle. The value of u_{min} for Case 2 is -47 m/s and T_{period} is 12 ms. Thus, the estimated distance, L_{rev}, is 199 mm.

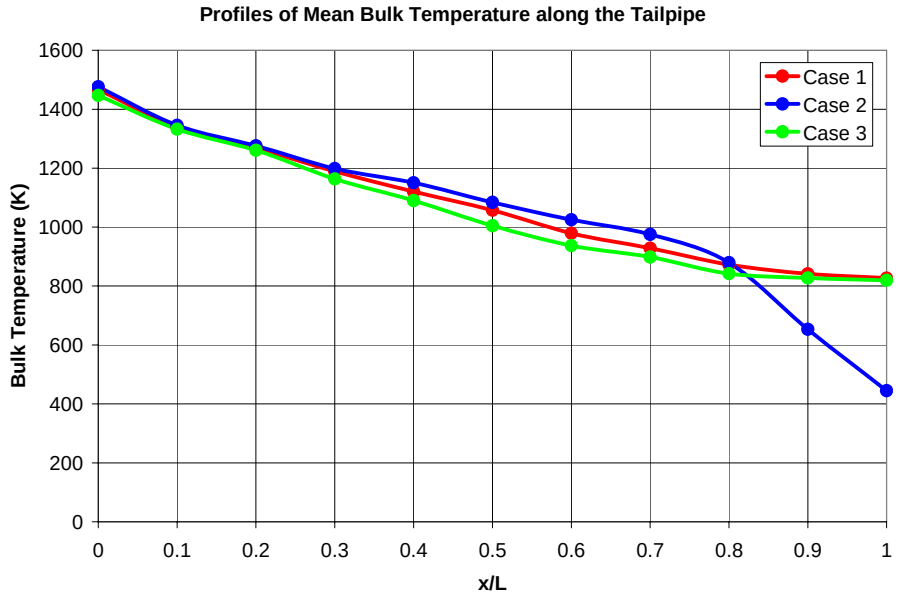

Figure 4.24: Mean bulk temperature profiles – All cases

Figure 4.25 shows the profiles of time-averaged and oscillation amplitude of bulk velocities along the tailpipe for all three cases. First, consider the profiles of velocity amplitude. For Cases 1 and 2, the amplitude increases along the tailpipe, clearly displaying compressible flow characteristics. As an effect of cooler ambient air, the magnitude of velocity amplitude from Case 2 is less than that from Case 1 everywhere in the tailpipe. For Case 3, the values of velocity amplitude remain relatively constant along most part of the tailpipe, behaving like an incompressible solid-plug flow. The profiles of velocity amplitude in Figure 4.25 will be used later to compare with the solutions of the linear acoustic theory and the simplified momentum equation.

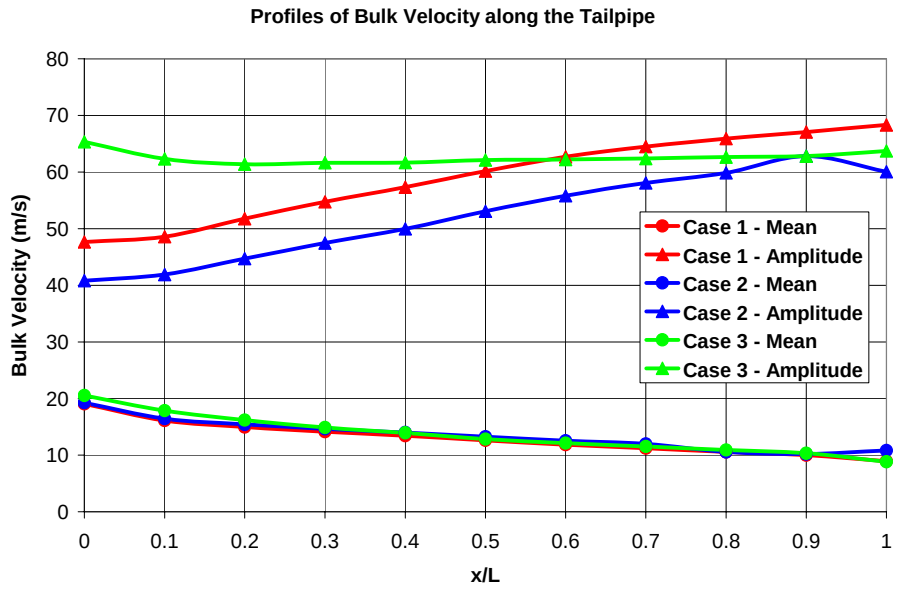

Figure 4.25: Mean and amplitude profiles of bulk velocity – All cases

Next, consider the profiles of mean velocity. Although Case 2 has significantly lower temperature at the exit than Case 1, the time-averaged velocities of these two cases

are almost the same. From the observation of instantaneous data of bulk velocities and temperatures in both cases, the time-averaged velocities correspond to maximum temperatures, not time-averaged temperatures. The maximum temperatures, at the tailpipe exit, are 875 and 933 K, for Cases 1 and 2, respectively. These values correspond to the time-averaged temperatures of fresh hot fluid that will be driven out of the tailpipe in each cycle. This is the fluid in the area just upstream from the location where ambient air reached during flow reversal. This behavior could be explained by the conservation of mass. As for periodically oscillating flows, instantaneous mass flow rate does not have to be equal everywhere along the tailpipe. However, the time-averaged mass flow rate over one cycle must be equal everywhere, as shown in Figure 4.26. The amplitude of mass flow rate oscillation is determined by the minimum velocity and the maximum value of density during the oscillation. At the tailpipe exit of Case 2, the ambient temperature is the lowest (300 K). During flow reversal, the mass flux, as the product of velocity and density, entering the tailpipe is, therefore, highest, as shown in Figure 4.26. In order to maintain the same mean positive mass flux, this reversed mass flux must be driven out of the tailpipe within the cycle. Then the rest of the cycle is used for driving the fresh hot gas with the amount of time-averaged mass flow rate out of the tailpipe. In other words, the oscillating part of velocity is responsible for mass flux amplitude (or the oscillating part of mass flux) which corresponds to maximum density. The oscillating parts of mass flux during the positive and negative cycle would cancel each other out. The mean velocity is responsible for mean mass flux that corresponds to the density of fresh hot fluid from upstream. The reason why the mean temperature is much lower than temperature from upstream is that the cooler mass flux is passing through the cross-

sectional area in both directions for longer than half the cycle, from the time starting to flow in until the time flowing back out. If the mean velocity corresponded to the mean temperature, the mean velocity would be low in Case 2, i.e., approximately 5 m/s, corresponding to the mean temperature of 444 K. In such case, the mean mass flow rate would be too low. The relation between the phase of velocity and temperature oscillations explained above could be observed from Figures 4.16 and 4.17 for Case 1 and Figures 4.18 and 4.19 for Case 2.

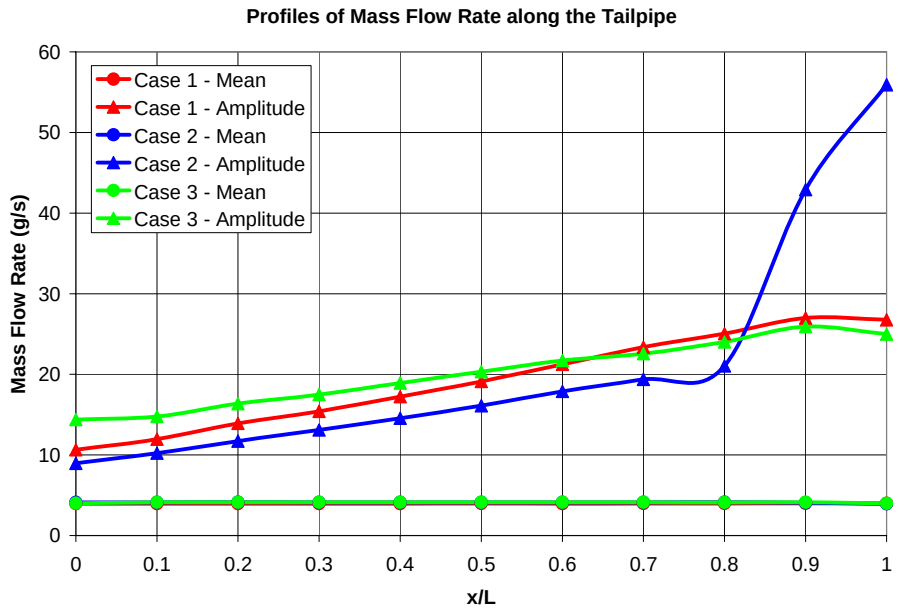

Figure 4.26: Mean and amplitude profiles of mass flow rate – All cases

Figure 4.27 shows the profiles of time-averaged and amplitude of pressure along the tailpipe. The mean pressure at the inlet, as a driving force of the whole mass in the tailpipe, is greater in Case 2 than in Case 1 due to greater amplitude of mass flow rate in Case 2. In addition, for a similar reason, the pressure amplitude gradient in Case 2 is

greater near the exit than upstream. And, as the pressure amplitude at the inlet is forced to be the same, the pressure amplitude gradient in Case 2 is less than Case 1 in the region near the inlet. As for Case 3, both mean pressure and pressure amplitude profiles are approximately the same as Case 1, which are approximately linear. This implies that the pulsating flow in the tailpipe of the Helmholtz pulse combustor, as qualitatively predicted in Figure 2.2, behaves more closely to an incompressible pulsating flow, although not pure solid-plug flow, than to a pure acoustic resonance in a Schmidt or quarter-wave tube. In other words, the pulsating flow in the Helmholtz pulse combustor tailpipe behaves like the pulsating flow near the open end of a Schmidt tube, i.e., in this portion, the gradient of pressure amplitude profile is close to linear and the velocity amplitude profile is close to constant (not starting from zero). Note that the mean pressure and the pressure amplitude at the tailpipe exit in Figure 4.27 were not zero, possibly because the atmospheric pressure was fixed at the "outlet" boundary instead of at the tailpipe exit.

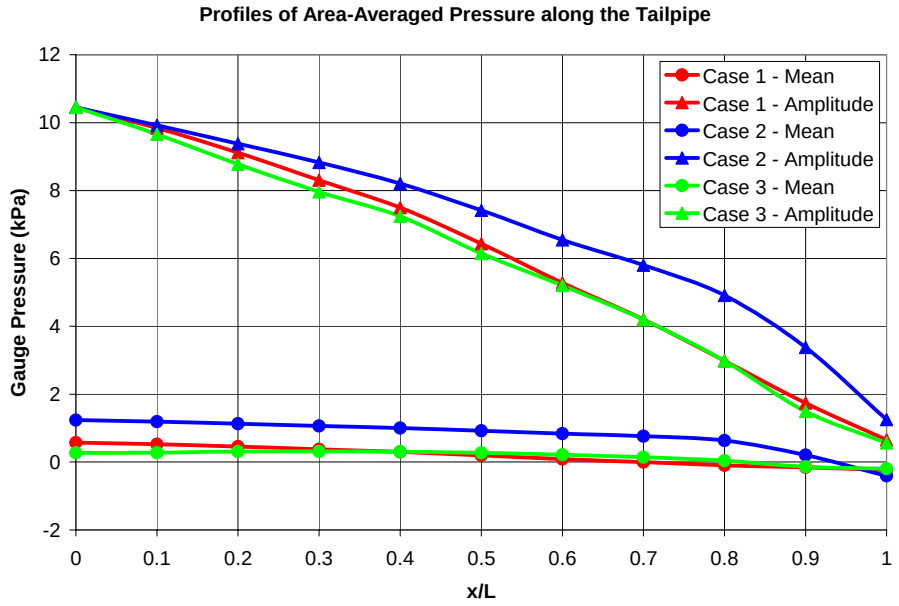

Figure 4.27: Mean and amplitude profiles of pressure – All cases

For another view on the effect of the cooler ambient air, temperature within the tailpipe was mass-flux-averaged for two halves, separately, and for the whole tailpipe. The plots of the oscillation for Cases 1 and 2 are shown in Figure 4.28. The first half (inlet side) of the tailpipe is generally not affected by the ambient air. For the second half (exit side) of the tailpipe, the variation in temperature of Case 2 is, as expected, much greater than Case 1. Overall, the time- and volume-averaged temperature is lower in Case 2 than in Case 1. Both instantaneous and time-averaged values of mass-flux-averaged temperature correspond well with the values of volume-averaged density, also collected from the simulation, with the calculation from the ideal gas law. Therefore, the mean values of mass-flux-averaged temperature for the whole tailpipe will be used in the approximations of the velocity amplitude in the next section.

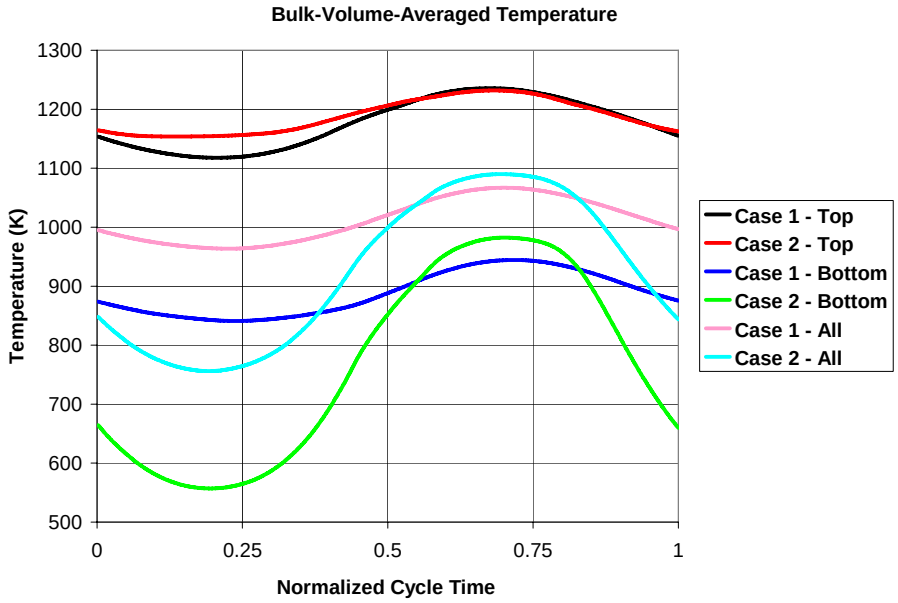

Figure 4.28: Bulk-volume-averaged temperature oscillation – Cases 1 and 2

For the summary in this section, the major finding was that the mean velocities did not correspond with the mean temperatures evaluated at the same positions, but corresponded to the maximum values of the temperature oscillations. This was most obvious at the tailpipe exit of Case 2, where the ambient temperature was room temperature. The cooler ambient air brought the mean temperature at the tailpipe exit down to 444 K, compared to 827 K in Case 1. Nevertheless, the mean velocity was still at the same level as that in Case 1. From mass conservation and the observation of the phase between temperature and velocity oscillations, the mean value of velocity oscillation was responsible for the mean mass flow rate, corresponding to the higher temperature of fluid upstream. And the oscillating part of velocity was responsible for the oscillating part of mass flow rate, in which the amplitude depended on the value of maximum density associated with lowest temperature downstream.

Velocity Amplitude Approximation

For bulk quantities, pulsating flow variables in a pipe could be approximated by assuming frictionless one-dimensional flow. From experimental results in the reference and simulation results, the behavior of a Helmholtz pulse combustor tailpipe flow is in between an incompressible flow and an acoustic resonance flow in a quarter-wave tube. In other words, although the pressure amplitude profile is almost linear, the velocity amplitude still increases to some extent along the tailpipe. Therefore, the linear acoustic theory should be more accurate than the solid-plug flow assumption in terms of profiles along the tailpipe. Nevertheless, the solid-plug flow assumption will still be used to estimate the velocity amplitude since the whole fluid flow in the tailpipe could be considered as a moving solid mass unit. In this section, three solutions of simplified one-

dimensional flow equations are compared with the solutions of CFD simulation. The comparison focuses on the profiles of the amplitude of velocity and pressure along the tailpipe.

The first approximation equation is the simplest form, based on the assumption of an incompressible frictionless solid-plug flow. This assumption considers the flow in the tailpipe as a single mass driven by the pressure gradient as a driving force. The pressure gradient is assumed to be linear. The governing equation for this assumption is the Euler's momentum equation:

$$\frac{\partial u}{\partial t} = -\frac{1}{\rho}\frac{\partial p}{\partial x}.$$

With additional assumptions that the solution is periodic and the mean pressure (gauge) is zero, the solution of the velocity amplitude can be derived as

$$u_A(x) = \frac{p_0}{\rho_m \omega L}, \tag{4.2}$$

where p_0 is pressure amplitude in the combustion chamber, ρ_m is mean density in the tailpipe, ω is radian frequency, and L is tailpipe length. The key parameter is the mean density, which should be a time- and space-averaged value over the whole tailpipe. In this thesis, the mean density is calculated from the mean mass-flux-averaged temperature in the tailpipe volume with the ideal gas law. The values of mean density from this calculation are about the same as the mean volume-averaged values of density from CFD solutions in Cases 1 and 2. The profile of the pressure amplitude for this approximation is simply a linear profile:

$$p_A(x) = p_0\left(1 - \frac{x}{L}\right). \tag{4.3}$$

The second approximation approach is based on the linear acoustic theory. A simple case of acoustic resonance in a tailpipe is a quarter-wave tube, in which pressure amplitude decreases sinusoidally from maximum at the inlet to zero at the exit whereas the velocity amplitude increases sinusoidally from zero at the inlet to the maximum at the exit. However, although the velocity amplitude of a Helmholtz pulse combustor is at maximum at the tailpipe exit, the velocity amplitude at the entrance is not zero, due to the finite volume of the combustion chamber. Therefore, some modification must be made to estimate a reasonable velocity amplitude profile. A straightforward method is to take a quarter of the acoustic wavelength, calculated from the actual frequency and the mean speed of sound, for the effective length of the tailpipe. Another method is to take the combustion chamber as an extended tailpipe length with an equivalent volume to the actual volume of the combustion chamber. From the actual dimension of the pulse combustor in the reference (the volume ratio was approximately 1.1) and the calculated wavelength ($\lambda = c_m/f$) from simulation results, where the mean speed of sound is calculated from the mean value of mass-flux-averaged temperature in the tailpipe volume (Figure 4.28), the extended tailpipe lengths from these two approaches are approximately the same. However, the pressure data of a Helmholtz pulse combustor is the pressure in the combustion chamber, which is usually taken as the pressure at the entrance of the tailpipe. Therefore, the pressure amplitude used for the calculation in the extended tailpipe must be modified so that the pressure amplitude at the point where the actual tailpipe begins is equal to the actual combustion chamber pressure amplitude. Then, the velocity amplitude profile of the actual tailpipe portion from the extended length is at the

last section with the actual tailpipe length. With this concept, the equation of the velocity amplitude profile for this extended tailpipe length is

$$u_A(x) = \frac{p_1}{\rho_m c_m} \sin\left(\frac{2\pi\left(x + \lambda/4 - L\right)}{\lambda}\right), \tag{4.4}$$

where $p_1 = \dfrac{p_0}{\sin\left(\dfrac{2\pi L}{\lambda}\right)}$ is the pressure amplitude at the beginning of the extended tailpipe, and p_0 is the pressure amplitude in the actual combustion chamber. ρ_m and c_m are calculated from the mean mass-flux-averaged temperature in the tailpipe volume. And the equation for the pressure amplitude profile is

$$p_A(x) = p_1 \cos\left(\frac{2\pi\left(x + \lambda/4 - L\right)}{\lambda}\right). \tag{4.5}$$

Finally, the third approach for the velocity amplitude approximation is to apply the linear acoustic theory and to impose a reasonable boundary condition at the entrance of the tailpipe. Ahrens (1979) applied the conservation of mass between the combustion chamber and the inlet of the tailpipe as the boundary condition. The details of the derivation of the acoustic wave equation solutions are given in the Appendix. The final solutions for the velocity and pressure amplitude profiles are

$$u_A(x) = \frac{p_0}{\rho_m c_m}\left[\cos\left(\bar{\omega}\bar{x}\right)/\tan(\bar{\omega}) + \sin(\bar{\omega}\bar{x})\right], \tag{4.6}$$

$$p_A(x) = p_0\left[\cos\left(\bar{\omega}\bar{x}\right) - \sin(\bar{\omega}\bar{x})/\tan(\bar{\omega})\right], \tag{4.7}$$

where $\bar{\omega} = \dfrac{\omega L}{c_m}$ and $\bar{x} = \dfrac{x}{L}$.

After plugging in all the numbers of parameters, it turns out that numerical values for the velocity amplitude profiles from the Equations (4.4) and (4.6) are exactly the same. Likewise, the values for the pressure amplitude profiles from Equations (4.5) and (4.7) are exactly the same. Thus, the two approaches with the linear acoustic theory are mathematically identical and have the same physical meaning. For the comparison with the CFD simulation, Equations (4.2) and (4.3) are referred to as "solid-plug" and Equations (4.4) - (4.7) are referred to as "acoustic."

Note that, in the acoustic theory, the value of L in Equations (4.4) – (4.7) should be an effective length, which is equal to the actual tailpipe length plus a length correction for an open-end tube. The length correction is also applied with a Helmholtz resonator, where the flow in the neck is assumed incompressible (Pierce, 1981). The length correction depends on the type of the open end, i.e., flanged or unflanged, which is equivalent to with or without a confined wall, respectively, in jet impingement geometry. Common values for the length correction are $0.85a$ and $0.6133a$, for flanged and unflanged tubes, respectively, where a is the radius of the tube (Blackstock, 2000). The flow geometry in this thesis is a flanged tube, thus the length correction is 0.85*17 = 14.45 mm. However, as the length correction is only 1.6% of the actual tailpipe length, the length correction is not added to the tailpipe length for the approximations of velocity and pressure amplitude in this thesis.

The results from the approximations of the velocity amplitude profiles together with the simulation results are shown in Figures 4.29 and 4.30, for Cases 1 and 2, respectively. The values of the solid-plug profiles are space-averaged values of the acoustic profiles. Thus, the velocity amplitude from the incompressible assumption is

higher at the tailpipe inlet and lower at the tailpipe exit, compared to the velocity amplitude profile from the acoustic assumption. The profiles from the linear acoustic theory are qualitatively accurate, compared to the solutions from CFD simulation. The magnitude of the estimated profiles is slightly overpredicted. Nevertheless, the profiles could be regarded as a fair and quick approximation, compared to the full model of CFD simulation. The most important parameter in these approximations is the mean bulk temperature in the whole volume of the tailpipe because this parameter is not easily measured in the experiments. This parameter leads to other parameters, i.e., mean density and mean speed of sound. Therefore, in order to have a fair approximation of velocity amplitude, an accurate value or at least a good approximation of the mean temperature must be obtained.

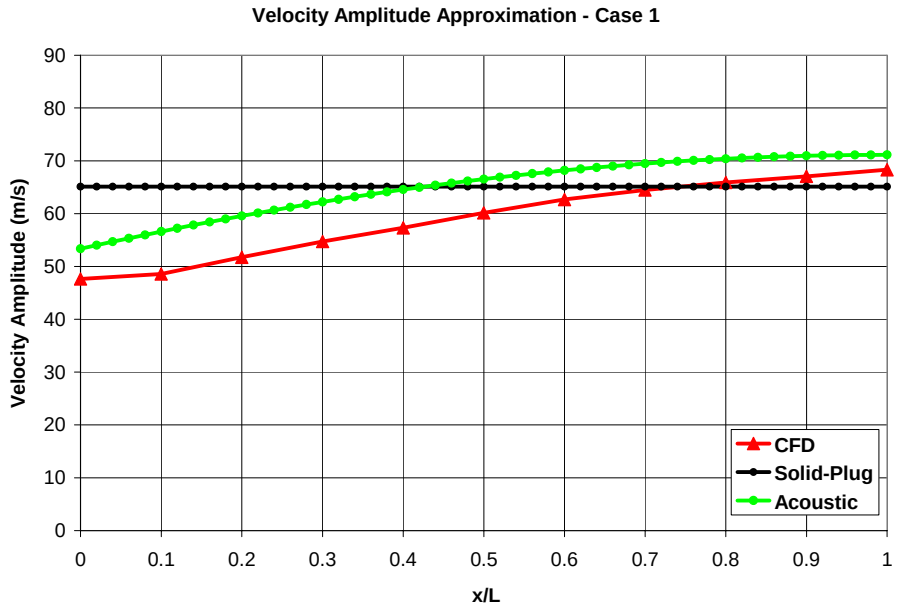

Figure 4.29: Approximation of velocity amplitude profiles – Case 1

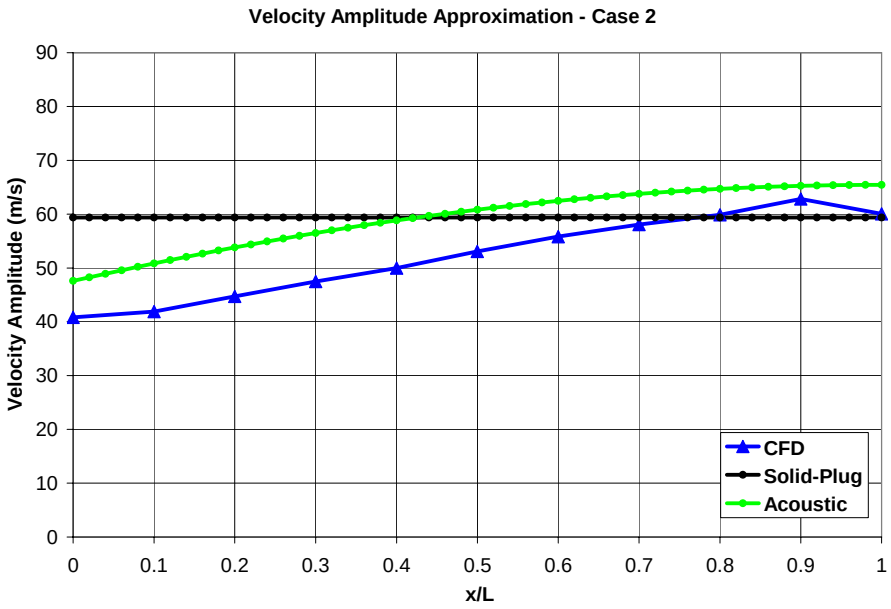

Figure 4.30: Approximation of velocity amplitude profiles – Case 2

Note that the approaches for approximating of velocity amplitude presented here are based on the assumption that the mean velocity is zero. This is only for the calculation purpose. In practice, the approximated velocity amplitude is usually superimposed on the actual mean velocity to obtain the complete velocity oscillation and the velocity amplitude ratio. The other note here is that the values of mean density used for calculating the velocity amplitude and the mean velocity are not necessarily the same. As discussed earlier, the mean density for the velocity amplitude should be the time-averaged and volume-averaged density in the tailpipe. For the mean velocity, also as discussed earlier, the density should correspond to the high temperature of the fluid upstream from the position where the velocity is evaluated.

In the Appendix, the derivation of Ahrens' solutions could predict the system frequency of a Helmholtz pulse combustor from the volume ratio of the combustion

chamber and the tailpipe. According to this prediction, the velocity amplitude estimated from the solid-plug assumption will be close to that from the acoustic solution when the volume ratio is larger than one. If the volume ratio is much smaller than one, the magnitude from the solid-plug assumption will be significantly lower than the magnitude from the acoustic solution. As an example, in a Schmidt pulse combustor, where the volume ratio is zero and the tailpipe length is a quarter of the acoustic wavelength, the magnitude of velocity amplitude ratio at the tailpipe exit could be accurately predicted by the linear acoustic theory, i.e., $p_A/(\rho_m c_m) = p_A/(\rho_m 4Lf)$. In this case, the magnitude from the incompressible Equation (4.2), $p_A/(\rho_m 2\pi Lf)$, will be lower than the acoustic magnitude by a factor of $2/\pi$. As the volume ratio increases, the magnitude from the incompressible assumption approaches the magnitude from the acoustic assumption, as shown in Figure 4.31. Solutions from both assumptions are very close when the volume ratio is much larger than one.

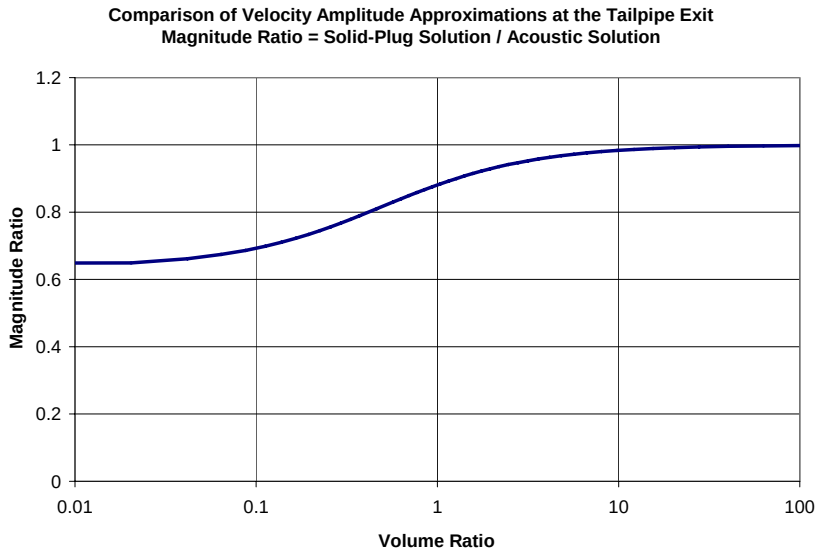

Figure 4.31: Comparison of velocity amplitude approximations at the tailpipe exit

For the experiments in the reference, the volume ratio of the pulse combustor was approximately 1.1. That possibly is the reason why the solid-plug assumption was a good approximation in this case. However, this analysis and the approximation of velocity amplitude profiles as well as the prediction of the relationship between the volume ratio and the frequency still needs to be verified with wider ranges of experimental data. Unfortunately, such data are not available. Therefore, the approximation of velocity amplitude in experiments, such as the drying experiment in Liewkongsataporn et al. (2006b), with this theory must be carefully applied. The analysis of the approximation method of the velocity amplitude in Liewkongsataporn et al. (2006b) was also based on an incompressible flow assumption, using two different density values at the two ends of the tailpipe. However, the conditions (no wall heat transfer) were different from the study cases in this thesis. Therefore, such an approach is not considered here.

The profiles of pressure amplitude along the tailpipe from the approximation equations are plotted in Figures 4.32 and 4.33, for Cases1 and 2, respectively, together with the results from CFD simulation. The profiles from the acoustic theory are close to linear because the extended length is longer than the actual tailpipe length, i.e., about 2 m vs. 0.88 m. The approximation of the pressure amplitude profiles is acceptable for Case 1, where the temperature oscillation at the tailpipe exit is relatively small. As for Case 2, where the oscillations of temperature and mass flow rate at the tailpipe exit are relatively large due to low ambient temperature, neither the acoustic theory nor the incompressible assumption could accurately predict the profile. Note that the pressure amplitudes at the tailpipe exit from the CFD solutions were not zero due to the atmospheric pressure condition at the “outlet” boundary. If the pressure amplitudes calculated by the

approximation methods at the tailpipe exit were adjusted to be equal to the values from the CFD solutions, the profiles should be in even better agreement, especially for Case 1.

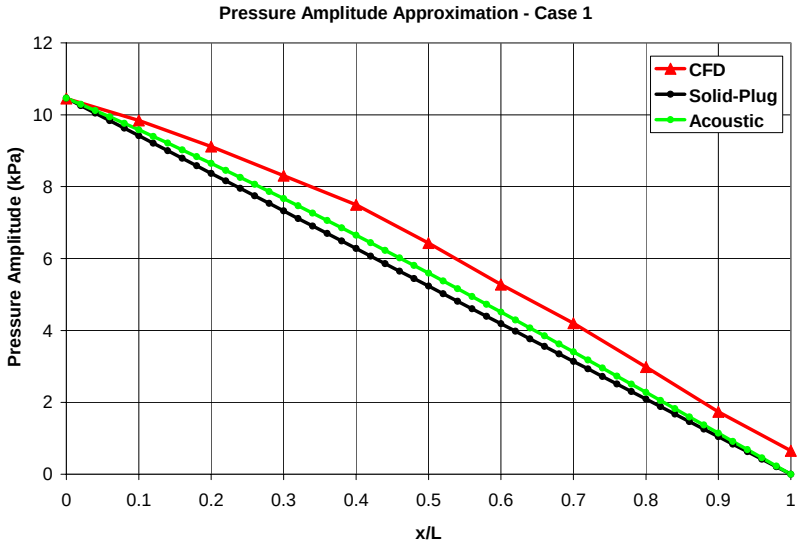

Figure 4.32: Approximation of pressure amplitude profiles – Case 1

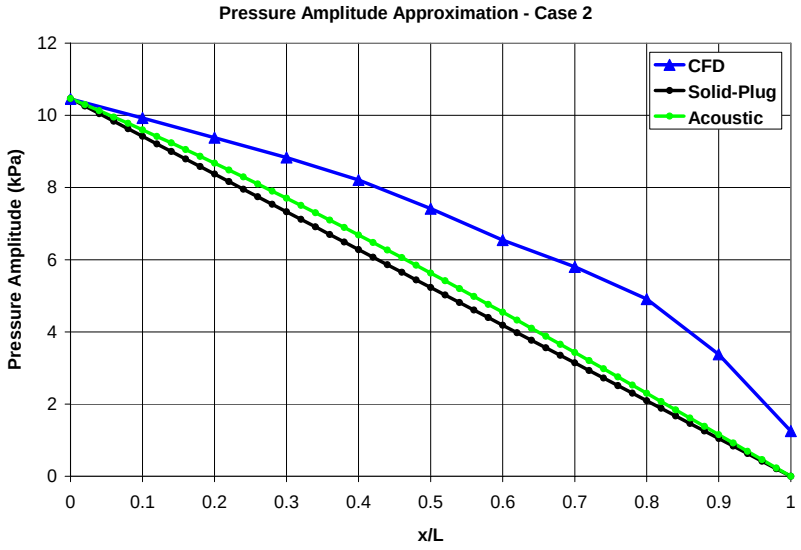

Figure 4.33: Approximation of pressure amplitude profiles – Case 2

For the summary of the velocity amplitude approximation, the linear acoustic theory with appropriate assumptions could be applied to estimate the profiles of velocity amplitude along the tailpipe. Overall, the acoustic approximation was qualitatively accurate. As for the quantitative accuracy, the acoustic solution was a fair approximation. The incompressible solid-plug assumption could also be used for the approximation, with a slight loss in accuracy. According to the prediction of the acoustic solutions in the Appendix, the velocity amplitude from this solid-plug assumption was only close to the acoustic approximation when the volume ratio was larger than one. However, the analysis and comparison in this section was done with only two cases of CFD simulation. More experimental data, if available, should be used to further verify the degree of the accuracy of the approximation.

CHAPTER 5

CONCLUSIONS AND RECOMMENDATIONS

The motivation of this thesis is the potential application of using a pulse combustor for enhancing the drying rate with respect to a conventional steady-jet impingement drying system. The PAD project at IPST has been investigating this application. CFD simulation has been used in numerical experiments for parameter studies. An objective of this thesis is to evaluate the solutions of the numerical simulation of pulsating tailpipe flows with available experimental data in the literature. Another objective is to study the effects of ambient temperature on the characteristics of pulsating flows.

Published data from the experiments of a Helmholtz pulse combustor at Sandia National Laboratories were used as reference for the results of numerical simulation. A CFD software package, FLUENT was used to simulate three study cases. Cases 1 and 2 were run with the ideal-gas law for density function. The experimental variable for these two cases was ambient temperature: 850 and 300 K, for Cases 1 and 2, respectively. Case 3 was run with a temperature-dependent polynomial function for the density. The ambient temperature for Case 3 was the same as Case 1. Three sets of computational grid were generated. Grid 1 was used for a preliminary study. Grids 2 and 3 were used for a grid independence study. Grid 2 was selected for final results presented and discussed in this thesis.

The flows were assumed axisymmetric. The computational domain began at the entrance of the tailpipe as the “inlet” of the domain. The exit of the tailpipe connected

with a large impingement zone with a wall extended from the tailpipe exit parallel to the impingement surface, with the "outlet" of the domain away from the tailpipe exit in the radial direction. The inlet boundary condition was pressure oscillation with an amplitude value from the reference. The outlet boundary condition was atmospheric pressure with backflow temperatures as ambient temperatures of the study cases. The turbulence model used in the simulation was the V2F model, which has been shown to be appropriate for complex flows such as strongly separated flows or unsteady three-dimensional flows.

Compared with data in the reference, results from Case 1, as a validation case, showed similar characteristics even though some conditions were simplified for the simulation. The main characteristic was the increase in velocity amplitude along the tailpipe, as expected for compressible flows. As for the effect of cooler ambient temperature on flow characteristics, results from Cases 1 and 2 were compared. The profile of mean temperature along the tailpipe was affected only within a short distance from the tailpipe exit. This distance corresponded to the furthest distance that ambient air could travel during flow reversal. Within this distance, the amplitude of mass flux oscillation was much greater in Case 2 than in Case 1. For the overall effects, Case 2 had higher mean pressure at the tailpipe inlet and lower velocity amplitude along the tailpipe than Case 1.

An interesting finding was mean velocities along the tailpipe from Cases 1 and 2 were at the same level even at the tailpipe exit, where the mean temperature in Case 2 was significantly lower than in Case 1. It was found that the mean velocity corresponded to the maximum value of the temperature oscillation cycle, not the mean value. This behavior still satisfied mass conservation. The oscillation part of velocity was responsible

for the oscillating part of mass flux, in which the magnitude of oscillation amplitude corresponded to maximum density during the oscillation. This would explain why the mass flow rate oscillation at the tailpipe exit in Case 2 was the largest compared to Case 1 or any other locations in Case 2. The mass flux that flowed back into the tailpipe must be driven out or cancelled out within one cycle so that the rest of the oscillation cycle could maintain the same mean mass flow rate along the tailpipe. This part was responsible for the mean velocity corresponding with fresh hot gas from upstream.

The approximation of velocity amplitude profiles were calculated with two simplifying assumptions: incompressible solid-plug flow assumption and the linear acoustic theory, which was modified from the theory for a quarter-wave resonance tube to incorporate the finite chamber volume. The magnitudes of the profiles from the solid-plug flow assumption were constant everywhere in the tailpipe, whereas the profiles from the acoustic theory were similar to the fully-compressible CFD solutions, i.e., increasing along the tailpipe. For the study cases in this thesis, the estimated velocity amplitudes from the two assumptions could be regarded as a fair approximation to the full-model CFD solutions. To be more exact, the magnitudes of approximated velocity amplitude profiles were slightly greater than the CFD solutions. One could argue that if more appropriate values of two parameters, i.e., the mean density and the mean speed of sound, are used, the profiles will be in better agreement. For example, the value of pressure used to evaluate the mean density from the ideal gas law could be higher than the atmospheric pressure used in this thesis. However, the comparison was based on only one set of operating conditions of a Helmholtz pulse combustor and on the numerical simulation.

Therefore, the methods of the approximation as well as the evaluation of the parameters should be further verified with wider ranges of experimental data.

Recommended future work is to apply mass flux oscillation at the "inlet" boundary and compare to the results with pressure oscillation, for the purpose of simplification of numerical simulation. The mean and amplitude of mass flux oscillation could be obtained from the results in this thesis. If the results are similar, the inlet mass flux oscillation would be a more convenient boundary condition for future numerical studies of pulsating jet impingement heat transfer because the key variable, the velocity amplitude ratio at the exit of the tailpipe, can be easily predetermined for the design of numerical experiment or a parameter study. Furthermore, the grid independence study would be easier because the mean mass flow rate would be exactly the same for each grid.

In experimental studies of impingement drying or heat transfer, simplified methods for estimating the mean velocity and the velocity amplitude at the tailpipe exit must be used carefully. The key variable for the approximation is temperature along the tailpipe. Although the data of pressure oscillation in the combustion chamber, mean mass flow rate, oscillation frequency, and tailpipe length are easily measured in the experiments, the data of temperature oscillation are much more difficult to measure. Usually, only mean temperature along the tailpipe is obtained. From the results of this thesis, the approximations of the mean velocity and the velocity amplitude require different information from temperature data. For the mean velocity, the value of mean temperature from upstream must be used instead of mean temperature at the tailpipe exit. For the velocity amplitude, the value of mean mass-flux-averaged temperature over the

whole tailpipe volume is recommended. Unless this quantity is properly measured, it is difficult to accurately calculate from the mean temperature profile because it requires the data of mass flux oscillation along the tailpipe as well. Therefore, the value of this parameter must be carefully evaluated.

For the numerical study of pulsating impingement heat transfer in the PAD project, the numerical results in this thesis offer two recommendations. First, pulsating flows in a tailpipe should be treated as compressible flow. In other words, the density function in the simulation, in which the computational domain covers the tailpipe, or a portion of the tailpipe, should be the ideal gas law because, compared to a temperature-dependent density function, the solutions not only are more physically accurate but they also converge faster. Second, the effects of grid generation, especially near-wall grid sizes, on numerical solutions should be investigated in more detail. As mentioned earlier, if the sizes of grid cells near walls are too small, instability in solutions could occur with the V2F turbulence model combined with the segregated solver. At this point, it is not clear whether the instability is a physical flow characteristic or is caused by the problem with the solver and the V2F model. The study of this behavior is important for pulsating impingement heat transfer because if the vortex-shedding like behavior is a physical characteristic, the number of toroidal vortices seen in Figure 4.21 could be more than one in an oscillation cycle. And these toroidal vortices could help in further enhancing impingement heat transfer by impinging onto the impingement surface independently from the pulsating core jet, thus providing an additional heat source to the impingement surface. On the other hand, if this behavior is a numerical instability problem, the grid generation should be performed with caution.

APPENDIX

DERIVATION OF AHRENS' ACOUSTIC SOLUTIONS

The underlying assumptions in the linear acoustic theory are that the rest state of fluid has zero velocity with constant pressure and speed of sound corresponding to the rest-state temperature and that the changes in pressure and density are very small compared the rest-state values. Therefore, the equations of mass and momentum conservation (inviscid) and the equation of state for an ideal gas can be linearized with the values in the rest state. Then these three linearized equations can be combined to obtain the linear wave equations of pressure change and velocity as well as velocity potential (Blackstock, 2000 and Pierce, 1981).

Equations (4.6) and (4.7) are solutions of the linear wave equations for a Helmholtz-type pulse combustor (with linearized compressible flow in the tailpipe) given in Ahrens (1979). The following is the derivation of the solutions according to Professor F. Ahrens.

The linear wave equations in the forms of pressure change and velocity potential are

$$\frac{\partial^2 p_f}{\partial t^2} = c_0^2 \frac{\partial^2 p_f}{\partial x^2} \tag{A.1}$$

$$\frac{\partial^2 \phi}{\partial t^2} = c_0^2 \frac{\partial^2 \phi}{\partial x^2} \tag{A.2}$$

$$p_f = -\rho_0 \frac{\partial \phi}{\partial t} \tag{A.3}$$

$$u_f = \frac{\partial \phi}{\partial x} \tag{A.4}$$

where $p_f = p\text{-}p_a$, $u_f = u\text{-}u_0 = u$, $p_f << p_a$, and $u << c_0$.

The boundary condition at the exit of the tailpipe ($x = L$) is a pressure node:

$$p_f(L,t) = 0 .$$

The boundary condition at the inlet of the tailpipe ($x = 0$) is the conservation of mass in the combustion chamber, assuming an isentropic process of an ideal gas:

$$\frac{V_c}{c_0^2}\frac{dp_f(0,t)}{dt} = -\rho_0 A_T u_f(0,t) .$$

where V_c is the volume of the combustion chamber and A_T is the cross-sectional area of the tail pipe.

Using dimensionless parameters, $\tau = \frac{c_0 t}{L}$ and $\xi = \frac{x}{L}$, Equation (A.2) becomes

$$\frac{\partial^2 \phi}{\partial \tau^2} = \frac{\partial^2 \phi}{\partial \xi^2} .$$

For a periodic solution, it can be assumed that

$$\phi = \Phi(\xi)\cos(\bar{\omega}\tau) ,$$

where $\bar{\omega} = \frac{\omega L}{c_0}$.

Hence,

$$-\bar{\omega}^2 \Phi(\xi) = \frac{\partial^2 \Phi(\xi)}{\partial \xi^2} .$$

A general solution is

$$\Phi(\xi) = A\cos(\bar{\omega}\xi) + B\sin(\bar{\omega}\xi) .$$

With the boundary condition at the exit, $\Phi(1) = 0$ (arbitrary constant),

$$A + B\tan\overline{\omega} = 0\,. \tag{A.5}$$

The boundary condition at the entrance in the dimensionless form is

$$-\overline{\omega}^2\Phi(0) = \frac{1}{\overline{V}}\frac{\partial\Phi(0)}{\partial\xi},$$

where $\overline{V} = V_c/(A_T L)$. Thus,

$$A = -\frac{B}{\overline{\omega}\overline{V}}\,. \tag{A.6}$$

From Equations (A.5) and (A.6),

$$\overline{\omega}\tan\overline{\omega} = \frac{1}{\overline{V}} \tag{A.7}$$

$$\Phi(\xi) = B\left[\sin(\overline{\omega}\xi) - \tan\overline{\omega}\cos(\overline{\omega}\xi)\right]$$

$$\phi = B\left[\sin(\overline{\omega}\xi) - \tan\overline{\omega}\cos(\overline{\omega}\xi)\right]\cos(\overline{\omega}\tau).$$

From Equations (A.3) and (A.4),

$$p_f = -\frac{\rho_0 c_0\overline{\omega}}{L}B\left[\sin(\overline{\omega}\xi) - \tan\overline{\omega}\cos(\overline{\omega}\xi)\right]\cos(\overline{\omega}\tau)$$

$$u_f = \frac{\overline{\omega}}{L}B\left[\cos(\overline{\omega}\xi) + \tan\overline{\omega}\sin(\overline{\omega}\xi)\right]\sin(\overline{\omega}\tau).$$

At $\xi = 0$, $\tau = 0$,

$$p_f = p_A = \frac{\rho_0 c_0\overline{\omega}}{L}B\tan\overline{\omega}\,.$$

where p_A is the pressure amplitude in the combustion chamber. Thus,

$$B = \frac{p_A L}{\rho_0 c_0\overline{\omega}\tan\overline{\omega}}\,.$$

Therefore, the final solutions are (Ahrens, 1979)

$$p_f = p_A\left[\cos(\bar{\omega}\xi) - \frac{\sin(\bar{\omega}\xi)}{\tan\bar{\omega}}\right]\cos(\bar{\omega}\tau) \tag{A.8}$$

$$u_f = \frac{p_A}{\rho_0 c_0}\left[\frac{\cos(\bar{\omega}\xi)}{\tan\bar{\omega}} + \sin(\bar{\omega}\xi)\right]\sin(\bar{\omega}\tau). \tag{A.9}$$

From Equation (A.7), two limiting cases of the volume ratio, $\bar{V}$, can be analyzed:

1. $\bar{V} \to 0$: $\bar{\omega} \to \frac{\pi}{2}$ and $\tan\bar{\omega} \to \infty$

$$p_f = p_A\cos\left(\frac{\pi\xi}{2}\right)\cos\left(\frac{\pi\tau}{2}\right) = p_A\cos\left(\frac{2\pi x}{\lambda}\right)\cos\left(\frac{2\pi c_0 t}{\lambda}\right)$$

$$u_f = \frac{p_A}{\rho_0 c_0}\sin\left(\frac{\pi\xi}{2}\right)\sin\left(\frac{\pi\tau}{2}\right) = \frac{p_A}{\rho_0 c_0}\sin\left(\frac{2\pi x}{\lambda}\right)\sin\left(\frac{2\pi c_0 t}{\lambda}\right)$$

$$\lambda \equiv \frac{c_0}{f} = 4L.$$

2. $\bar{V} \to \infty$: $\tan\bar{\omega} \to \bar{\omega} \to \frac{1}{\sqrt{\bar{V}}}$, $\sin(\bar{\omega}\xi) \to \bar{\omega}\xi$, $\cos(\bar{\omega}\xi) \to 1 - \frac{(\bar{\omega}\xi)^2}{2}$

$$\bar{\omega} \to \frac{\omega_s L}{c_0} = \bar{\omega}_s = \frac{1}{\sqrt{\bar{V}}} \tag{A.10}$$

where ω_s is the radian frequency of a Helmholtz resonator:

$$\omega_s = c_0\sqrt{\frac{A_T}{V_C L}} = \frac{c_0}{L\sqrt{\bar{V}}}$$

$$p_f = p_A(1-\xi)\cos\left(\frac{\omega_s L\tau}{c_0}\right) = p_A\left(1 - \frac{x}{L}\right)\cos(\omega_s t)$$

$$u_f = \frac{p_A}{\rho_0 c_0 \bar{\omega}}\sin(\bar{\omega}\tau) = \frac{p_A}{\rho_0 \omega_s L}\sin(\omega_s t).$$

The first case is the solution of a Schmidt or quarter-wave resonance tube. The second case is the solution of a Helmholtz resonator, where the flow in the tailpipe (neck) is usually assumed incompressible. The solutions in the second case are the same as Equations (4.2) and (4.3). Figure A.1 shows the relation of the system frequency and the volume ratio predicted by Equation (A.7) compared with the theory of a Helmholtz resonator, Equation (A.10). The second limit case, where the volume ratio is very large, is clearly demonstrated in Figure A.1.

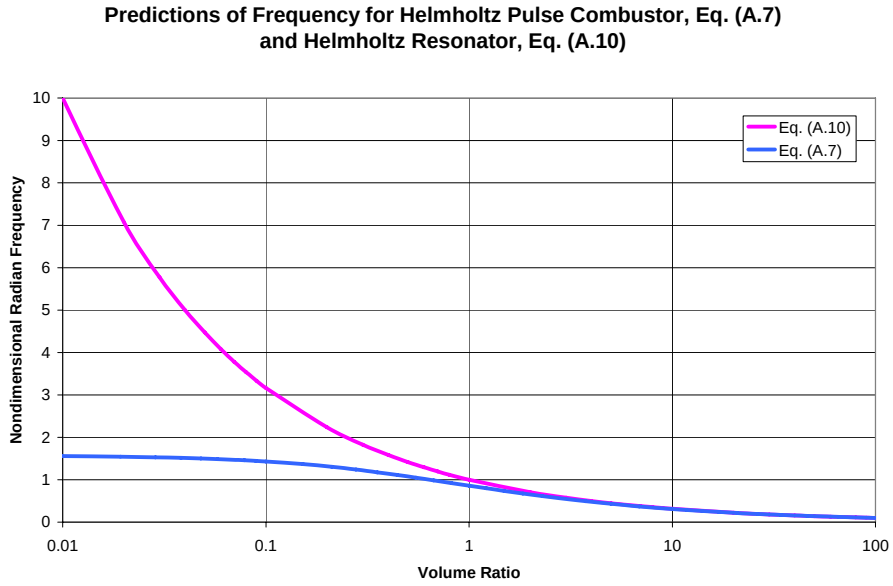

Figure A.1: Prediction of system frequency for Helmholtz pulse combustor and Helmholtz resonator (reproduced from Ahrens, 1979)

REFERENCES

Ahrens, F. W. (1979). Prediction of heat transfer in pulse-combustion burners. In *Proceedings of the Symposium on Pulse Combustion Technology for Heating Applications*, Argonne, Illinois, pp. 46-66.

Behnia, M., Parneix, S., and Durbin, P. A. (1998). Prediction of heat transfer in an axisymmetric turbulent jet impinging on a flat plate. *International Journal of Heat and Mass Transfer*, Vol. 41, No. 12, pp. 1845-1855.

Behnia, M., Parneix, S., Shabany, Y., and Durbin, P. A. (1999). Numerical study of turbulent heat transfer in confined and unconfined impinging jets. *International Journal of Heat and Fluid Flow*, Vol. 20, pp. 1-9.

Bird, R. B., Stewart, W. E., and Lightfoot, E. N. (2002). Transport Phenomena, 2nd Edition, John Wiley & Sons, New York.

Blackstock, D. T. (2000). Fundamentals of Physical Acoustics, John Wiley & Sons, New York.

Dec, J. E. and Keller, J. O. (1989). Pulse Combustor Tail-Pipe Heat-Transfer Depedence on Frequency, Amplitude, and Mean Flow Rate. *Combustion and Flame*, Vol. 77, pp. 359-374.

Dec, J. E. and Keller, J. O. (1990). Time-Resolved Gas Temperatures in the Oscillating Turbulent Flow of a Pulse Combustor Tail Pipe. *Combustion and Flame*, Vol. 80, pp. 358-370.

Dec, J. E., Keller, J. O., and Hongo I. (1991). Time-Resolved Velocities and Turbulence in the Oscillating Flow of a Pulse Combustor Tail Pipe. *Combustion and Flame*, Vol. 83, pp. 271-292.

Durbin, P. A. (1991). Near-Wall Turbulence Closure Modeling Without "Damping Functions." *Theoretical and Computational Fluid Dynamics*, Vol. 3, pp. 1-13.

Durbin, P. A. (1995). Separated Flow Computations with the k-ε-v^2 Model. *AIAA Journal*, Vol. 33, No. 4, pp. 659-664.

Eibeck, P. A., Keller, J. O., Bramlette, T. T., and Sailor, D. J. (1993). Pulse Combustion: Impinging Jet Heat Transfer Enhancement. *Combustion Science and Technology*, Vol. 94, pp. 147-165.

Etemad, S. and Sundén, B. (2006). Numerical investigation of turbulent heat transfer in a rectangular-sectioned 90° bend. *Numerical Heat Transfer, Part A*, Vol. 49, pp. 323-343.

FLUENT 6.1 υ^2-f Turbulence Model Manual (2003). Fluent Inc.

FLUENT 6.2 User's Guide (2005). Fluent Inc.

Hanby, V. I. (1969). Convective Heat Transfer in a Gas-Fired Pulsating Combustor. *Journal of Engineering for Power*, Vol. 91, No. 1, pp. 48-52.

Incropera, F. P. and DeWitt, D. P. (2002). Fundamentals of Heat and Mass Transfer, 5th Edition, Wiley, New York.

Keller, J. O., Eibeck, P. A., Bramlette, T. T., and Barr P. K. (1993). Pulse Combustion: Tailpipe Exit Jet Characteristics. *Combustion Science and Technology*, Vol. 94, pp. 167-192.

Keller, J. O. and Barr, P. K. (1996). Premixed Combustion in a Periodic Flow Field. In *Unsteady Combustion*, Eds., Culic, F., Heitor, M. V., and Whitelaw, J. H., Kluwer Academic Publishers, Netherlands, pp. 17-32.

Kudra, T. and Mujumdar, A. S. (2002). Advanced Drying Technologies., Marcel Dekker, New York.

Laurence, D. R., Uribe, J. C., and Utyuzhnikov, S. V. (2004). A Robust Formulation of the v2-f Model. *Flow, Turbulence and Combustion*, Vol. 73, pp. 169-185.

Liewkongsataporn, W., Ahrens, F., and Patterson, T. (2006a). A numerical study of axisymmetric pulsating jet impingement heat transfer. To be presented at *the 13th International Heat Transfer Conference*, Sydney, Australia, August 13-18, 2006.

Liewkongsataporn, W., Patterson, T., Ahrens, F., and Loughran, J. (2006b). Impingement drying enhancement using a pulsating jet. To be presented at *the 15th International Drying Symposium*, Budapest, Hungary, August 20-23, 2006.

Lodahl, C. R., Sumer, B. M., Fredsoe, J. (1998). Turbulent combined oscillatory flow and current in a pipe. *Journal of Fluid Mechanics*, Vol. 373, pp. 313-348.

Manna, M. and Vacca, A. (2005). Resistance Reduction in Pulsating Turbulent Pipe Flows. *Journal of Engineering for Gas Turbine and Power*, Vol. 127, pp. 410-417.

Parneix, S., Durbin, P. A., and Behnia, M. (1998). Computation of 3-D Turbulent Boundary Layers Using the *V2F* Model. *Flow, Turbulence and Combustion*, Vol. 60, pp. 19-46.

Pierce, A. D. (1981). Acoustics: An Introduction to Its Physical Principles and Applications, McGraw-Hill, New York.

Pikulik, I. I. (1994). High-Intensity Drying of Paper. In *Proceedings of the 80th Annual Meeting,* Technical Section, CPPA, Montreal, Canada, pp. A11-A23.

Schilichting, H. and Gersten, K. (2000). Boundary Layer Theory, 8th Edition, Springer-Verlag, Germany.

Scotti, A. and Piomelli, U. (2001). Numerical simulation of pulsating turbulent channel flow. *Physics of Fluids*, Vol. 13, No. 5, pp. 1367-1384.

Scotti, A. and Piomelli, U. (2002). Turbulence Models in Pulsating Flows. *AIAA Journal*, Vol. 40, No. 3, pp. 537-544.

Sujith, R. I., Waldherr, G. A., and Zinn, B. T. (1995). An exact solution for one-dimensional acoustic fields in ducts with an axial temperature gradient. *Journal of Sound and Vibration*, Vol. 184, No. 3, pp. 389-402.

Unsal, B., Ray, S., Durst, F., and Ertunc, O. (2005). Pulsating laminar pipe flows with sinusoidal mass flux variations. *Fluid Dynamics Research*, Vol. 37, pp. 317-333.

Wang, X. and Zhang, N. (2005). Numerical analysis of heat transfer in pulsating turbulent flow in a pipe. *International Journal of Heat and Mass Transfer*, Vol. 48, pp. 3957-3970.

Zinn, B. T. (1996). Pulse Combustion Applications: Past, Present and Future. In *Unsteady Combustion*, Eds., Culic, F., Heitor, M. V., and Whitelaw, J. H., Kluwer Academic Publishers, Netherlands, pp. 113-137.

Zuckerman, N. and Lior, N. (2005). Impingement Heat Transfer: Correlations and Numerical Modeling. *Journal of Heat Transfer*, Vol. 127, pp. 544-552.